PCCP

Accepted Manuscript

ROYAL SOCIETY OF CHEMISTRY

www.rsc.org/pccp

Length Dependence of Electron Transport through Molecular Wires – A First Principles Perspective

Khoong Hong Khoo [a,b,c], Yifeng Chen [a,b], Suchun Li [a,c,d] and Su Ying Quek [a,b,*]

[a] Department of Physics, Faculty of Science, National University of Singapore, 2 Science Drive 3, Singapore 117551, Singapore
[b] Graphene Research Center, National University of Singapore, 6 Science Drive 2, Singapore 117546, Singapore
[c] Institute of High Performance Computing, Agency for Science Technology and Research, 1 Fusionopolis Way, #16-16 Connexis, Singapore 138632, Singapore
[d] NUS Graduate School for Integrative Sciences and Engineering, National University of Singapore, 28 Medical Drive, Singapore 117456

[*]e-mail: phyqsy@nus.edu.sg

Abstract

One-dimensional wires constitute a fundamental building block in nanoscale electronics. However, truly one-dimensional metallic wires do not exist due to Peierls distortion. Molecular wires come close to being stable one-dimensional wires, but are typically semiconductors, with charge transport occurring via tunneling or thermally-activated hopping. In this review, we discuss electron transport through molecular wires, from a theoretical, quantum mechanical perspective based on first principles. We focus specifically on the off-resonant tunneling regime, applicable to shorter molecular wires (< ~4-5 nm) where quantum mechanics dictates electron transport. Here, conductance decays exponentially with the wire length, with an exponential decay constant, beta, that is independent of temperature. Different levels of first principles theory are discussed, starting with the computational workhorse – density functional theory (DFT), and moving on to many-electron GW methods as well as GW-inspired DFT+Sigma calculations. These different levels of theory are applied in two major computational frameworks – complex band structure (CBS) calculations to estimate the tunneling decay constant, beta, and Landauer-Buttiker transport calculations that consider explicitly the effects of contact geometry, and compute the transmission spectra directly. In general, for the same level of theory, the Landauer-Buttiker calculations give more quantitative values of beta than the CBS calculations. However, the CBS calculations have a long history and are particularly useful for quick estimates of beta. Comparing different levels of theory, it is clear that GW and DFT+Sigma calculations give significantly improved agreement with experiment compared to DFT, especially for the conductance values. Quantitative agreement can also be obtained for the Seebeck coefficient – another independent probe of electron transport. This excellent agreement provides confirmative evidence of off-resonant tunneling in the systems under investigation. Calculations show that the tunneling decay constant beta is a robust quantity that does not depend on details of the contact geometry, provided that the same contact geometry is used for all molecular lengths considered. However, because

conductance is sensitive to contact geometry, values of beta obtained by considering conductance values where the contact geometry is changing with the molecular junction length can be quite different. Experimentally measured values of beta in general compare well with beta obtained using DFT+Sigma and GW transport calculations, while discrepancies can be attributed to changes in the experimental contact geometries with molecular length. This review also summarizes experimental and theoretical efforts towards finding perfect molecular wires with high conductance and small beta values.

Main text

The field of molecular electronics has seen remarkable progress during the past few decades. The vision of using molecular components for electronics applications has been proposed back in the 1970s [1, 2], and experimental advancements such as scanning probe techniques and break junctions have provided the necessary tools for the fabrication and characterization of these molecular electronic devices.

Molecular wires, which are usually understood as one-dimensional rod-like molecular structures made from single molecules or their assemblies, constitute one of the most important building blocks of molecular electronics. Typical molecular wires studied extensively in the literature include oligo(phenylene ethynylene)s (OPEs), oligo(phenylene vinylene)s (OPVs), oligo-thiophenes, oligo-phenyls, oligoynes, oligoacenes, oligo-porphyrins, DNA, and alkane chains [3-11]. Electron transport studies through these molecular wires are particularly important for both understanding their fundamental properties from a scientific perspective and guiding their utilization in practical devices, such as in molecular circuits, organic solar cells, organic light-emitting diodes (OLED), and organic field-effect transistors (OFET) [12, 13]. π-conjugated molecular wires are usually more conductive, hence they are often proposed as potential linking structures in molecular circuits. On the other hand, saturated molecular wires like alkane chains have higher resistance, but are less susceptible to extrinsic effects in experimental measurements, which makes them suitable for fundamental studies.

In this review, we focus on the study of electron transport through molecular wires, from a first principles perspective. That is, we shall discuss methodologies that treat the electron transport problem by solving Schrodinger's equation, without any empirical parameters but with some well-defined approximations.

The paper is organized as follows. Section 1 provides a general introduction to transport through molecular wires, including phenomena that are not typically studied using first principles methodologies. In section 2, we begin our focus on first principles studies, providing a background for the first principles methods involved in the study of electron transport across molecular wire junctions. In section 3, we present detailed examples of these first principles methods applied to different molecular wire systems and compare results with experimental measurements. In section 4, we summarize different transport characteristics within the tunneling regime for a number of different wire systems, in efforts towards understanding and predicting perfect molecular wires.

Section 5 presents concluding remarks, including some future perspectives on problems which still remain open in the field.

1. Introduction and Background

Earlier studies of molecular electronics systems started with molecular assemblies such as Langmuir-Blodgett (LB) films or self-assembled monolayers (SAMs) [14-16]. These ingeniously synthesized molecular assemblies routinely reach single-molecule thicknesses. Sandwiched between a back electrode and top metal contacts or probes, electron transport through these systems can be systematically studied in experiments, providing the first results at the single-molecular level. Although short-range intermolecular interactions are usually not negligible in these monolayer systems, results from SAMs or LB films are routinely used to provide insight into truly single-molecular junctions wherever appropriate. Device contacting and measuring strategies usually include nanopores, nanoparticle top contacts, conducting-probe atomic force microscopy (CP-AFM), crossed wire junctions, mercury drop junctions, and conducting polymer top contacts [17].

For single molecular systems, an experimental breakthrough came during the late 1990s, when M. A. Reed *et al.* [18] first used mechanically controlled break junctions (MCBJs) to successfully obtain electron conductance data through a molecular benzenedithiol (BDT) system sandwiched between two gold electrodes. This method subsequently became one of the most important fabrication techniques for single-molecule electronic devices. Besides MCBJs, electrochemical break junctions (BJs) and scanning tunneling microscopy (STM) based BJs were also developed by several groups to investigate molecular systems in solution [19, 20]. STM-BJs have the advantage that they can be repeatedly formed and broken over numerous cycles very easily.

However, interpretation of results from single-molecule experiments is usually non-trivial. Initially, discrepancies between theory and experiments and between experiments from different groups were prevalent. Eventually, it was realized that various effects such as device contact geometry, metal/molecule interfaces, molecular anchoring and side groups, inelastic effects, molecular conformation, and stochastic fluctuations can all influence experimental results considerably [21-29]. A statistical analysis method was employed by Xu and Tao [30] to unambiguously determine transport characteristics through single molecular junctions. By constructing a conductance histogram using data from thousands of molecular junctions formed between a gold STM tip and gold substrate, well-defined histogram peaks were identified at integer multiples of a fundamental conductance value (usually a small fraction of G_0 for alkanedithiol systems). The lowest conductance histogram peak is interpreted to correspond to single molecular junctions while higher conductance peaks are attributed to junctions having multiple molecules linking the gold electrodes. This kind of statistical analysis has subsequently become a standard procedure in data analysis for single molecule experiments.

In spite of the seminal work by Xu and Tao, subsequent experiments by numerous groups on alkanedithiol-Au junctions still find qualitatively different conductance histograms from previous results. These differences have since been attributed to variations in the atomic configurations of the thiol-gold bonds and changes in the conformation of alkane molecules [31, 32]. The strong dependence of conductance on molecular conformation has also been observed in phenyl molecules. Experimental studies by L. Venkataraman *et al.* [26] have demonstrated a $\cos^2\theta$ conformational dependence of the electron conductance through a series of diamine-biphenyl junctions at various twist angles θ, consistent with theoretical predictions.

Although the thiol anchoring group is popular in the literature for single molecular systems because it readily forms strong bonds with metallic electrodes, it also suffers from serious shortcomings, such as high variability of conductance with details of the junction geometry, hindering junction reliability and measurement reproducibility. Other anchoring groups used for molecular wire studies include amine, nitro, cyano, pyridine, carboxyl, and heterocycle groups as well as molecules directly bound to the contacts [20, 33-35]. In particular, the amine anchoring group is found to bind preferentially with under-coordinated gold atoms, enabling well-defined conductance characteristics for single molecular devices, even though the coupling of amines with metallic contacts is usually weak [20].

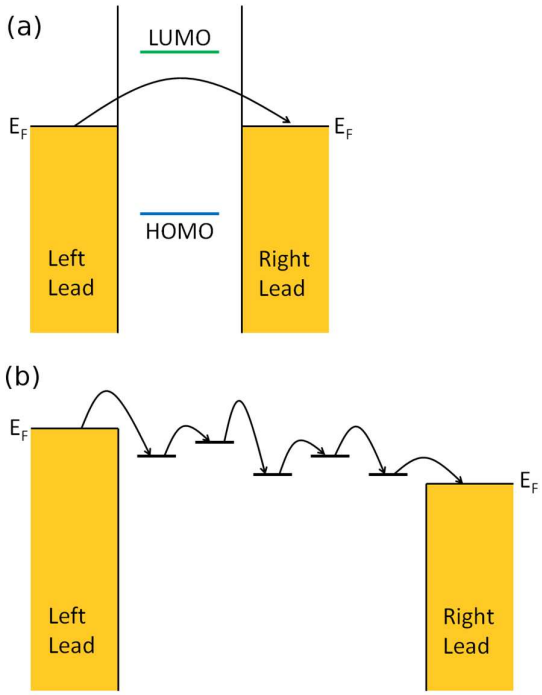

Figure 1. Schematic illustration of the coherent off-resonant electron tunneling mechanism (a) and the multi-step electron hopping mechanism (b) through molecular wire bridges sandwiched between two electrodes.

Electron transport mechanisms in molecular wire junctions can largely be classified into two categories, coherent tunneling and incoherent hopping, with a length-dependent mechanism crossover between the two regimes [36].

For short or saturated wires with large E_F-LUMO (or HOMO, whichever is closer) separation, the dominant transport mechanism is a one-step coherent off-resonant tunneling of the carriers through the molecular bridge, as shown in Figure 1(a). In the coherent off-resonant tunneling regime, inelastic effects such as electron-phonon couplings do not significantly affect the room temperature conductance of single molecules. Since the molecular wire bridge effectively acts as a guiding barrier for the charge carriers to tunnel through, the differences between electron tunneling through molecular assemblies versus single molecular wires are less significant. In particular, through-molecule tunneling has been found to be dominant over through-space tunneling (tunneling between molecules in the SAM) [37].

For longer conjugated molecular wires under moderate temperatures, there will be localized sites on the bridge where charge carriers can temporarily reside; the longer bridge length means that carriers need to spend more time on the molecules, which subsequently increases the chances of coupling with molecular vibrational modes. Furthermore, it is easier to distort backbones and excite or absorb vibrational modes in longer wires. Thus the dominant transport mechanism here changes into a multi-step incoherent hopping of carriers from site to site on the bridge, as shown in Figure 1(b). The inter-site hopping transition is usually believed to be thermally-activated, following the Marcus picture of electron transfer.

There are substantial characteristic differences between tunneling and hopping transport mechanisms. For coherent off-resonant tunneling transport, the electron conductance (resistance) usually displays an exponentially decreasing (increasing) behavior with respect to the bridge length L:

$$G = G_c e^{-\beta L} \quad \text{or} \quad R = R_c e^{\beta L} \quad (1)$$

Here G_c (R_c) is the contact conductance (resistance) of the molecular wire junction, while β is the tunneling decay constant that depends on the molecular backbone. Also, tunneling transport is largely temperature independent.

For incoherent hopping transport, junction resistance increases linearly with the bridge length:

$$R \propto \alpha L \quad (2)$$

where α usually shows an Arrhenius-type thermal activation behavior. Hence in hopping transport, there is a strong temperature dependence of the transport properties. The linearly increasing resistance behavior of longer conjugated molecular wires is akin to electron transport through intrinsic conductive polymers, and the length-dependent crossover from tunneling to hopping has also been observed in intramolecular electron transfer processes of a donor-bridge-acceptor system [38]. Identifications of the correct transport mechanism and accurate predictions of both current magnitudes and transport characteristics are vitally important for the understanding and device applications of molecular wire systems. For example, short conductive molecular wires with a small tunneling decay factor β like the recently synthesized Au-C direct bonding wires [39, 40], could be used as perfect connectors between functional components in molecular electronic circuits, while π-conjugated long oligomers or polymers within the

incoherent hopping transport regime are important for applications such as organic solar cells, OLED, or OFET.

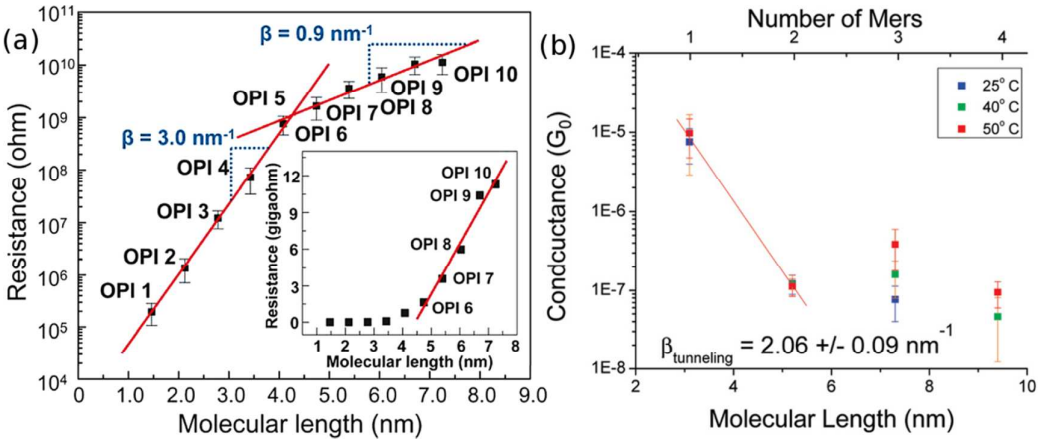

Figure 2. (a) CP-AFM measured electron resistance data of OPI molecular wires with respect to their lengths in a semi-log plot. Insert: Linear scale plot. (b) STM-BJ measured electron conductance of one group of conjugated single molecular wire junctions from 1-mer to 4-mer in a semi-log plot. (Panel (a) is reproduced by permission of the American Association for the Advancement of Science (ref. [41])). (Panel (b) is reproduced by permission of the American Chemical Society (ref. [42])).

For electron transport through molecular wire systems, the transition from tunneling to hopping mechanism has been observed for both molecule assemblies and single molecular systems. Choi *et al.* [41] used the CP-AFM method to measure the length-dependent transport of a set of oligo-phenyleneimine (OPI) SAMs with lengths ranging from 1.5 to 7.3 nm. The resistance data taken from averages of I-V traces were plotted as shown in Figure 2(a). The transition point can be clearly identified at OPI 5 where the wire length is about 4 nm. The linearly increasing behavior of molecular resistance from OPI 6 to OPI 10 shown in the inset indicates the onset of hopping dominated transport for longer wires. These conclusions are also corroborated by temperature-dependence measurements in the same report. In another study, Hines *et al.* [42] used the STM-BJ technique and investigated the length and temperature dependence of electron conductance through one group of conjugated single molecular wires ranging from 3.1 to 9.4 nm in length (1- to 4-mer). The collected data from conductance histograms are shown in Figure 2(b). The mechanism transition point is clearly determined as between 2-mer and 3-mer, which means a length between 5.2 and 7.3 nm. Temperature dependence studies also revealed strong conductance variations for longer 3, 4-mer wires, while showing no significant variation for shorter 1, 2-mer wires, consistent with the mechanism crossover picture.

Aside from electron conductance G or resistance R properties through nanoscale molecular wires, thermal transport and thermoelectric properties are emerging as new important research directions [43, 44]. In particular, the thermoelectric response across various types of molecular wires have been successfully measured from experiments and investigated from theory [45, 46].

As the focus of our present review is on a first principles perspective of electron transport, we now comment on which of the transport phenomena discussed above are amenable to first principles studies. Since first principles methods are inherently quantum mechanical, they are ideal tools for investigating electron transport in the coherent off-resonant tunneling regime. First principles methods can provide predictions of the tunneling decay factor β, and the conductance G at low finite biases. As long as transport is within the tunneling regime and not too far from equilibrium, first principles methods can also be used to predict the thermopower, or Seebeck coefficient S, in molecular wire junctions. Inelastic effects within the tunneling regime can also be treated using first principles within perturbation theory; we refer the reader to excellent reviews on this topic, in particular in relation to low temperature inelastic tunneling spectroscopy experiments [47-53]. On the other hand, incoherent hopping transport is rarely treated fully from first principles. As the reorganization energies in Marcus theory result from the rearrangement of solvent molecules in addition to geometric changes in the conducting molecule, first principles studies of such processes are computationally demanding. Instead, semi-empirical techniques are more commonly applied [13].

2. First Principles Methods

The workhorse of first principles calculations is density functional theory (DFT). However, an issue of DFT is the notorious underestimation of the HOMO-LUMO gap, owing to the fact that the Kohn-Sham eigenenergies are Lagrange multipliers with no physical significance. Since tunneling transport depends critically on the energy barrier, the inaccurate HOMO-LUMO gap can lead to serious quantitative errors, especially for the conductance G [54, 55]. The decay factor β and thermopower S are also affected by this error, although to a smaller extent. Despite these issues, DFT transport calculations can often still yield qualitatively meaningful results, as demonstrated in the studies on the geometry dependence of conductance [56-58]. One way to improve the DFT quasiparticle spectrum is to introduce a non-local energy dependent self-energy correction using the GW approximation [59, 60]. Transport properties computed using the GW approximation have significantly improved agreement with experiment [61, 62]. However, a drawback of this method is that it is computationally intensive and scales badly with system size, so that it can only be applied to systems having a small number of atoms. Recently, a "multiscale" method called DFT+Σ has been introduced to quantitatively predict conductance values at the same computational expense as DFT calculations [11]. The DFT+Σ method uses a DFT Hamiltonian, but corrects for inaccuracies in the molecular levels using a self-energy correction term based on GW calculations. This method is able to yield quantitatively accurate conductances, however, it is only applicable to systems where the molecular resonances are sufficiently far from the Fermi level so that the broadened resonance is either fully occupied or fully unoccupied, and where the polarizability of the molecule is sufficiently small [63, 64].

While DFT or GW tells us how to treat the electron-electron interactions in the many-body system, a theoretical framework is required in order to compute transport properties. The Landauer-Buttiker formalism allows one to directly compute the

transmission spectra of a two-electrode system, and is often the method of choice to compute the conductance G and thermopower S in molecular junctions. On the other hand, the decay constant β can also be estimated using simpler complex band structure (CBS) calculations.

Another promising framework for studying non-equilibrium transport, which we shall introduce only briefly here, is time dependent current-density functional theory (TDCDFT) that directly probes the time development of the system. Conductances of prototypical systems have been studied and a dynamical exchange–correlation correction to the conductance has been identified [65-67]. A complication of this method is that the Runge-Gross theorem, which underpins TDCDFT, is not proven for non-equilibrium open-systems. Possible workarounds include the use of large but finite leads [68, 69] or the inclusion of complex absorbing potentials that make the leads essentially finite [70]. In addition, currently available exchange-correlation potentials are unable to account for non-local effects, essential for accurately describing molecular conductance.

In the following, we introduce the CBS and Landauer-Buttiker formalisms, and finally provide a detailed description of the DFT+Σ method, which is used in the Landauer-Buttiker formalism.

2.1 Complex Bandstructure Calculations

For molecular wires, which consist of a set of repeating units, the tunneling decay constant β can be evaluated from the complex band structure (CBS) of the corresponding periodic polymer [71], computed by considering the energy E as input and solving for the set of wavevectors k that produce this energy for a given Hamiltonian. The output k-values are generally complex, and in particular, for E in the band gap of the polymer, the k-values are purely imaginary. At the interface between a metal and the polymer, incoming states from the metal decay as $e^{-Im[k(E)]L}$ while their tunneling probability decays as $e^{-2Im[k(E)]L}$. Thus β can be obtained as $2Im[k(E_F)]$, where E_F is the Fermi energy of the metal. Such evanescent states within the band gap of the polymer, which originate from the adjacent metal, are known as metal-induced gap states.

A simple way of estimating the Fermi level lineup within the CBS was suggested by Tersoff [72]. In general, if the density of the metal-induced gap states is sufficiently large, the Fermi level should be pinned at the charge neutrality level (CNL), and this can be estimated to be at the branch point $\left(\frac{dE}{dk} \to \infty\right)$ within the band gap having the smallest Im(k), as shown in Figure 3(a). This method provides a reasonable first estimate of the Fermi level alignment.

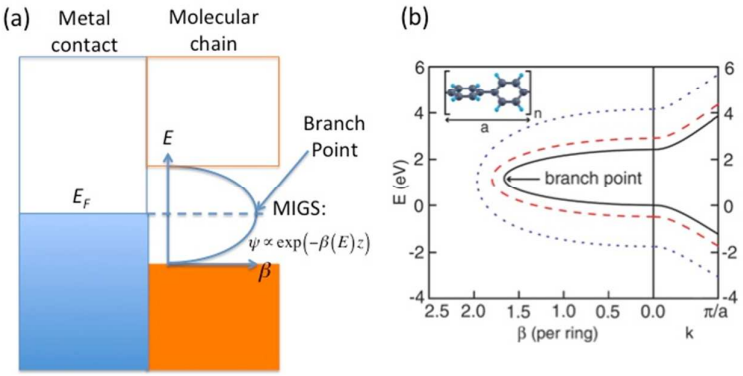

Figure 3. (a) Schematic of the molecule-contact interface including the imaginary part of the complex band structure. The Fermi level is typically pinned at the branch point within the band gap having the smallest Im(k). (b) Right (left) panels are real (imaginary) band structures of periodic chain with different band gaps E_g. Right: Highest valence and lowest conduction bands. Left: Complex band corresponding to the smallest imaginary k within the gap. The energy E is plotted against $\beta(E)=2a\mathrm{Im}(k_{min}(E))$. All other bands are explicitly omitted. Inset: Atomic geometry of a repeat unit of the periodic polyphenyl chain. (Panel (b) is reproduced by permission of the American Chemical Society (ref. [11])).

Compared to evaluating β from transport calculations involving the full molecular junction, such as in the Landauer-Buttiker formalism, the CBS method has the advantage that it is more direct and computationally efficient. Also, the CBS carries detailed information about the tunneling layer and its evanescent states, which makes it an interesting analysis and characterization tool. However, the CBS method does have several limitations. The metal contacts, anchoring groups, and contact geometry can only influence β through the placement of the Fermi level within the CBS. This implicitly assumes that the interfacial interactions are not dominant. In addition, the band gap of the periodic polymer is usually smaller than the HOMO-LUMO gaps obtained for short oligomers. A possible solution to this is to add a 'scissor-shift' operator to the Hamiltonian when computing the CBS, as illustrated in the CBS for oligophenyls in Figure 3(b) [11]. However, this HOMO-LUMO gap is also generally length-dependent, especially for short molecules. Overall, the CBS method provides a reasonable estimate for the value of β, but it does lack quantitative accuracy that may be accessible through direct transport calculations. [11]

The above discussion has focused on extracting transport properties from the CBS. Alternatively, if the transmission spectra is known, one can also derive an "effective complex band structure" $\beta_{N,N'}(E)$ defined as $-\frac{1}{(N-N')}ln\left(\frac{T_N}{T_{N'}}\right)$ [11]. This function avoids the ambiguities of E_F alignments and represents a decay constant encompassing the physical features of the molecular junction. The effective CBS allows one to obtain information such as the sensitivity of β to differences in junction level alignment and also analyze contact-dependent features not available in regular CBS calculations.

2.2 Landauer-Buttiker Formalism

In mesoscopic systems where the length scale becomes comparable to electron wavelengths, quantum effects dominate electron transport. Landauer showed that for coherent transport in this regime, the conductance is closely related to the probability of electron transmission, and this is summarized in the following equation

$$G = \frac{2e^2}{h}\,\tau(E) = G_0\,\tau(E) \quad (3)$$

where G is the conductance, G_0 the conductance quantum, and $\tau(E)$ the transmission function. This formalism has been successfully applied to numerous mesoscopic and molecular systems.

In the linear response regime, when the thermally induced electrical voltage ΔV is proportional to the applied temperature difference ΔT, we can define the thermopower S as $S = -(\Delta V/\Delta T)|_{I=0}$ at the steady state zero current. Under conditions that the average junction temperature T is relatively small so that the electron transmission varies smoothly within k_BT of the Fermi level, and for ΔT much smaller than T, we can write the thermopower S in the following form

$$S = -\frac{\pi^2 {k_B}^2 T}{3e}\,\frac{\partial \ln(\tau(E))}{\partial E}\Big|_{E=E_F} = -S_0\,\frac{\partial \ln(\tau(E))}{\partial E}\Big|_{E=E_F} \quad (4)$$

where $\tau(E)$ is the transmission spectrum and k_B is the Boltzmann constant [73-75].

Starting from first-principles electronic structure methods such as DFT, the electron transmission spectrum can be computed either by the non-equilibrium Green's function (NEGF) method, as implemented in transport packages such as TranSIESTA [76] and SMEAGOL[77], or the scattering-state method as implemented in SCARLET [78, 79].

In these transport calculations, one first constructs an open-boundary system consisting of a left lead, right lead, and central resistive region. For the NEGF method, the retarded Green's function G^r of the resistive region is evaluated along with the self-energies of the leads. These quantities are then used to evaluate the transmission spectrum using the following expression

$$\tau(E) = Tr[\Gamma_L(E)G^a(E)\Gamma_R(E)G^r(E)] \quad (5)$$

where G^a is the advanced Green's function, obtained by taking the complex conjugate of G^r, and $\Gamma_{L/R}(E)$ are the coupling strengths of the left/right leads with the resistive region, evaluated from the imaginary parts of their self-energies. For the scattering state method, a matrix representation of the Kohn-Sham Hamiltonian is constructed and solved as a generalized eigenvalue problem, together with boundary matching at different parts of the two-probe setup. Wavefunctions of scattering states incident from the probe into the resistive region are evaluated and used to obtain the transmission spectrum $\tau(E)$.

When a finite bias V is applied across the resistive region, a self-consistent procedure is employed to obtain the steady-state non-equilibrium transmission spectrum $\tau(E,V)$, and

the current-voltage (I-V) characteristics for electron transport is evaluated from the following integration

$$I(V) = \frac{2e}{h}\int_{-\infty}^{\infty} dE\ \tau(E,V)\left[f\left(E+\frac{eV}{2}\right) - f\left(E-\frac{eV}{2}\right)\right] \quad (6)$$

where f is the lead Fermi-Dirac distribution. Although DFT is inherently a ground state theory, DFT transport calculations at finite bias can often be interpreted qualitatively. Corrections to the DFT exchange-correlation functional have also been proposed for finite bias calculations. [80]; however, in this review, we will be focusing on conductance and thermopower values under quasi-equilibrium, zero-bias conditions.

Compared to the complex band structure method described previously, Landauer transport calculations are much more computationally intensive. However, the advantage is that one obtains not just the decay constant β, but also the contact conductance G. Also, these calculations account for the contact, anchoring groups, and variations in the junction geometry explicitly, all of which have been shown to have non-negligible effects in determining transport properties in single molecule junctions. The Landauer calculations are also much more general, and can be used to describe electron transport in other regimes, such as coherent resonant tunneling.

2.3 DFT, GW and DFT+Σ

The simplest physical picture of coherent off-resonant tunneling consists of electrons tunneling across a one-dimensional potential barrier V ($V > E$), with the tunneling decay constant given by $\beta \sim (2m(V-E))^{1/2}/\hbar$. A predictive theory for transport in single-molecule junctions thus relies on an accurate prediction of the tunneling barrier $E_{barrier} = V\text{-}E$, which is approximately given by the quasiparticle energy of the frontier molecular orbital relative to the Fermi level. The quasiparticle energy can be predicted accurately using the GW method [59, 60], which can be understood as being analogous to Hartree-Fock except that the screened Coulomb potential is used instead of the bare Coulomb potential. As such, GW considers the effect of electronic screening in response to the removal of an electron or hole from the system, in addition to exchange interactions that are already present in Hartree-Fock. On the other hand, DFT Kohn-Sham eigenvalues are introduced as Lagrange multipliers in the formalism, but are often used as a qualitative approximation to the quasiparticle energies. The actual value of the Kohn-Sham HOMO-LUMO gap depends on the flavor of the exchange-correlation potential used in the DFT calculation. Typically, the local density approximation (LDA) and generalized gradient-corrected approximations (GGA) give HOMO-LUMO gaps that are too small. Hybrid functionals [81, 82] that explicitly include a percentage of exchange interactions widen this gap, as do self-interaction corrections [83].

Several transport calculations have been performed explicitly in the GW framework, and these have resulted in significantly more accurate level alignments and conductance values compared to DFT [61, 84-86]. In addition, first-principles GW calculations have been used to provide physical insight into many-body and dynamical effects involved in image charge formation [87, 88]. Despite the success of the GW transport formalism, its high computational cost has prompted the development of a GW motivated parameter-

free self-energy operator on DFT that corrects for level alignments and predicts quantitatively accurate conductances within the single-particle picture [11, 35, 89]. This DFT+Σ method is inspired by studies performed by Neaton *et al.* to investigate the difference between GW and DFT LDA eigenvalues for the energy level alignment of physisorbed molecules on a metallic surface [90]. In addition to the underestimation of the HOMO-LUMO gap by DFT LDA, it was found that long-range correlation effects due to surface electrostatic screening of the metal electrodes leads to a substantial decrease of the HOMO-LUMO quasiparticle gap, shown schematically as $\Delta\Sigma_{\mathrm{LUMO}}$ and $\Delta\Sigma_{\mathrm{HOMO}}$ in Figure 4. This correction is completely missing from the corresponding Kohn-Sham gap, as can be seen in Table 1, where the GW HOMO-LUMO gap for benzene on graphite reflects variations in screening effects due to differences in the molecular environment, while DFT LDA yields a gap that is nearly constant. This lack of transferability to different environments is characteristic also of hybrid functionals in DFT, where the non-local nature of the exchange-correlation effect is not fully taken into account [90-93]. The results of Table 1 imply that for a physisorbed molecule on a metal substrate, the self-energy correction to the DFT HOMO and LUMO levels can be obtained as a sum of two parts: (1) the self-energy correction in the gas phase, which typically increases the HOMO-LUMO gap, and (2) the self-energy correction due to image charge effects in the substrate, which reduces the HOMO-LUMO gap. (Figure 4) This method has also been applied to benzenediamine on Au(111), and obtained excellent agreement with photoemission results [94]. The two-part self-energy correction in Figure 4 is also applicable to molecules chemisorbed on metal substrates, provided that the molecular resonances are sufficiently far from the Fermi level so that the broadened resonance is either fully occupied or fully unoccupied, and that the polarizability of the molecule is sufficiently small [63, 64].

	Gas Phase	Flat on Graphite	Crystal Phase
ΔE_{gap} (LDA)	5.16	5.05	5.07
ΔE_{gap} (GW)	10.51	7.35	7.91

Table 1. Benzene HOMO-LUMO gaps in the gas phase, crystal phase, and adsorbed on the graphite surface from ref. [90]. First and second lines are Kohn-Sham (LDA) and quasiparticle (GW) gaps. (Values for the crystal are averaged over the π and π* manifolds.) Energies are in eV.

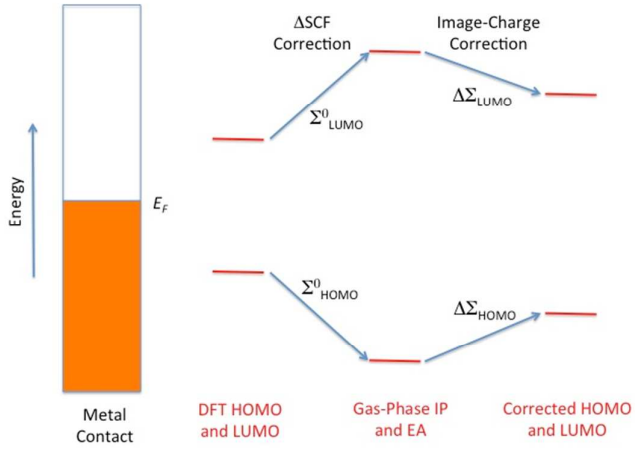

Figure 4. Two-part self-energy correction to DFT HOMO and LUMO levels for a molecule on a metal substrate. This correction applies to cases where the molecular resonances are sufficiently far from the Fermi level so that the broadened resonance is either fully occupied or fully unoccupied, and where the polarizability of the molecule can be neglected.

The gas-phase correction Σ^0_{HOMO} and Σ^0_{LUMO} can be easily obtained by comparing the DFT, HOMO and LUMO levels of the gas-phase molecule with the ionization potential (IP) and electron affinity (EA) computed from total energy differences within the ΔSCF method. The image-charge correction $\Delta\Sigma$ can be obtained using electrostatics and details are provided in the next subsection. Self-energy corrections for the metallic leads are usually small compared with the molecule, and can be safely neglected. Therefore, in order to correct for the self-energy errors in DFT, we can add to the DFT Hamiltonian a self-energy operator

$$\hat{\Sigma} = \sum_n \Delta_n |\psi_n^{mol}><\psi_n^{mol}| \quad (7)$$

where $|\psi_n^{mol}>$ denotes the n-th molecular orbital. In practice, Σ_{HOMO} is used for all occupied levels, and Σ_{LUMO} for all unoccupied levels, since only the HOMO and LUMO typically affect transport at the Fermi level. We note that in practice, the above formalism relies on the molecule remaining intact upon adsorption in the junction; further work is being carried out to include other classes of molecules.

DFT+Σ has been implemented for both NEGF [85] and scattering-state formalisms [11, 35, 89, 95]. In both cases, the charge density is first converged from transport calculations using standard-DFT XC functionals. The self-energy operator $\hat{\Sigma}$ is then added to the Hamiltonian and the calculation carried out in a "one-shot" non-self-consistent fashion based on the converged DFT charge density to obtain the transmission spectrum. This procedure has been shown to yield accurate molecule-contact level alignments and conductances for molecular systems satisfying the necessary conditions. DFT+Σ transport calculations have been shown to be equivalent to static GW transport calculations [88].

2.3.1 Image charge correction

Previous experimental [96] and theoretical work [90] have shown that image-charge effects are dominant in single-molecule junctions, and this leads to significant gap renormalization. A simple model for estimating the image-charge correction $\Delta\Sigma$ is to represent the added electron/hole as a single point charge in the middle of the molecule between two perfect parallel conducting surfaces. The energy associated with this configuration is given by $\Delta\Sigma = -\frac{e^2}{a} ln(2)$ using the method of images, where a is the electrode separation. Applying this formula to the benchmark case of Au-BDA junctions, and using an image plane position ~1Å from the Au surface, we obtain a $\Delta\Sigma^{HOMO}$ of ~+1 eV. Combining this with the bare HOMO self-energy correction of -3 eV yields a Σ^{HOMO} correction of -2 eV. This shift modifies the calculated conductance from 0.046 G_0 to 0.007 G_0, giving much better agreement with the experimental value of 0.0064 G_0 [58].

In actual DFT+Σ calculations, a more refined model is employed where the orbital charge density is represented by Mulliken charges centered on each atom. Here, the image charge correction is

$$\Delta\Sigma = -\frac{1}{2}\sum_{i,j=1}^{N} q_i \phi(q_j, r_i, r_j) \quad (8)$$

where q_i is the Mulliken charge on the ith atom and $\phi(q_j,r_i,r_j)$ is the potential at r_i due to the image charges of the Mulliken charge q_j on the jth atom. It has been found that typical values of $\Delta\Sigma$ calculated from Equation (8) are within 0.1 eV of that calculated from single-point-charge models for the benzene-diamine molecule. Another factor affecting $\Delta\Sigma$ is the image plane position, which is dependent on the response of the electrode surface to an applied field. This position can be obtained from first-principles DFT calculations following the procedure laid out by Lam and Needs [97].

3 Comparison between Calculations and Experiment

3.1 Complex Band Structure Calculations

In general, the CBS method has been used to investigate tunneling in a wide variety of molecular systems including alkanes [71, 98, 99], alkenes[71, 100], silanes [98], polyphenyls [11, 100], DNA strands [101], PPE [56, 71, 102], and carbon nanotubes [103]. In addition, there has also been a GW CBS study on alkanes, alkenes, PPE, and PPI molecules, with comparisons made to DFT local, semilocal, and hybrid-exchange density functionals [104]. It was found that local and semilocal density functionals systematically underestimate the β parameter, while hybrid-exchange schemes partially correct for this discrepancy, resulting in much better agreement with GW calculations and experiments.

CBS calculations of β have proven to be particularly predictive in the case of alkane chains. Experiments on alkane chains sandwiched between Au contacts have yielded a β of 0.94-1.07 [31, 105, 106] and 0.91 [20] per methyl group for thiol and amine terminated molecules respectively. Junctions where alkane molecules are directly linked to Au contacts have also been fabricated to give a β value of 0.97 [39]. Earlier DFT-CBS

calculations that align E_F using Tersoff's method have yielded β between 0.9-1.0 [71, 99], while a more recent DFT study utilizing the B3LYP hybrid-functional and E_F from junction calculations gives $\beta \sim 0.81$ and 0.93 per methyl group for Au-alkanedithiol and Au-alkanediamine junctions respectively [98]. It can be seen from these calculations that the anchoring group does not have a strong effect on the tunneling decay constant for alkane chains, and CBS calculations gives β values in fairly good agreement with experiment. The insensitivity of β to environmental factors and DFT errors, as well as to the exact placement of E_F, has been attributed to the large band gap of alkane chains producing a relatively flat CBS with nearly constant β over a broad energy range [107].

As for oligophenyls, another common class of molecular wires, the decay constant β for self-assembled monolayers (SAMs) of oligophenylene thiolates on Au substrates has been measured to be 1.8 per phenyl group [108]. Similarly, β for single oligophenyldiamine molecules sandwiched between Au and Ag contacts have been measured to be between 1.7-1.8 per phenyl ring [26, 109], while oligophenyls directly connected to Au leads give a higher value of 2.0 [40]. For oligophenyl chains, DFT-CBS calculations employing the Tersoff approach gives a β of 1.6 per phenyl group, slightly below the experimental range [100]. In another CBS study, a scissor shift was applied to match the CBS gap to the HOMO-LUMO band gap in oligophenyldiamine-Au junctions (a DFT+Σ type calculation) [11]. The Fermi level E_F is then placed above the VBM using E_F-HOMO alignments from molecular-junction calculations, giving a β of 2.0 per phenyl ring.

3.2 Landauer-Buttiker Transport Calculations

3.2.1 Conductance and β

As mentioned previously, DFT transport calculations on molecular junctions tend to overestimate conductances due to errors in the lineup of frontier molecular orbitals relative to the contact Fermi level. This is especially the case for off-resonant tunneling, where conductance is very sensitive to the energy barrier. We note that because DFT Kohn-Sham values do give qualitatively reasonable band structures, transport in the resonant and near-resonant regime tend to be quite well described by DFT transport calculations, even for molecular junctions, such as H_2 across Pt or Pd leads [4, 21, 110] or Nb-nanowire junctions [111]. Attempts to improve upon the level alignments to describe off-resonant tunneling transport include the use of self-interaction corrections [112], hybrid functionals [113], and scissor shift operators fitted to Hartree-Fock (HF) gaps [114]. Despite missing non-local correlation effects, these methods in general give better agreement with experiment than LDA or GGA transport calculations, because they widen the gap and therefore lower the conductance values. A reasonable conductance value was also obtained for molecular junctions containing BDT by considering scattering within the configuration interaction (CI) formalism [115], however concerns have been raised that the boundary conditions imposed in these calculations may lead to unphysical results [116].

Numerous transport studies invoking the GW approximation have been shown to predict accurate conductances [61, 62, 84-86, 117]. However, the poor scaling of many-body calculations with system size means that correlations can only be introduced in a

small calculation region, and it is necessary to use highly simplified representations of junction structures. This may present issues as the junction conductance has been shown to be sensitive to atomic structure [118-120].

Let us now consider studies on several prototypical single molecule junctions. Unless otherwise stated, DFT values reported from the literature are obtained within LDA or GGA.

Just as DFT CBS calculations have been particularly effective for predicting β in alkane chains, we see from Table 2 that DFT transport calculations are similarly effective. In contrast, the value obtained from higher-level CI calculations is clearly too small.

β of alkanedithiol-Au junctions per methyl group		
DFT	CI	Experiment
0.95 [121]	0.50 [122]	1.0±0.1 [105]
0.95-0.99 [123]		1.07±0.05 (MC), 1.07±0.05 (HC) [106]
1.24 [120]		0.94±0.05 (MC), 0.96±0.15 (HC) [31]
0.88 (MC), 0.83 (HC) [31]		
1.19 [124]		
β of alkanediamine-Au junctions per methyl group		
DFT	GW	Experiment
0.92 [84]	1.02 [84]	0.91±0.03 [20]
1.01 [98]		

Table 2. Experimental and theoretical tunneling decay constants β of alkanedithiol-Au and alkanediamine-Au junctions. HC and MC refers to the β corresponding to the high conductance and medium conductance families respectively. Units of β are given per CH_2-group.

It is interesting in particular to note that both the medium and high conductance families (corresponding to different contact geometries) in the alkanedithiol-Au junctions have very similar β values, although the conductances in the two families differ by a magnitude of ~5 [31]. This indicates that β is much less sensitive to contact geometry than actual conductance values, especially for the alkanedithiol molecules. Experimentally, three families of junctions with distinct conductance values have been found for these molecules, with each family corresponding to a different atomic configuration at the molecule-electrode bond [31, 32, 125-127]. DFT calculations on Au-alkanedithiol-Au junctions have also found a strong dependence of conductance on the binding geometry, consistent with the family behavior observed in experiments [120, 123]. In contrast to alkanedithiol-Au junctions, alkanediamine-Au junctions exhibit a unique contact conductance G_c instead of the family behavior observed for alkanedithiol junctions. This unique contact conductance comes from the fact the amine groups bind selectively to undercoordinated Au sites, while the thiol group can bind to different Au binding sites with very similar binding energies. Experiments have reported a G_c of

$0.030G_0$ [20] while DFT calculations predict a much larger value of 0.11 G_0 [84]. Introducing GW corrections brings G_c down to $0.04G_0$ [84], in very good agreement with experiment. Recently, metal-alkane junctions with direct Au-C bonding without anchoring groups were synthesized [128]. These junctions show almost a 100-fold increase in conductance relative to their thiol or amine linked counterparts due to the strong Au-C bonding. As mentioned previously, the decay constant β is found to be 0.97 ± 0.2 per carbon, which is similar to those obtained from experiments on alkane chains with anchoring groups. DFT based transport calculations indicate that the transmission at the Fermi level is dominated by the Au-C σ–bonding orbitals. With its unambiguous bonding geometry and high conductance, it would be interesting to investigate transport through these junctions from first-principles with proper self-energy corrections.

Moving on to discuss the conjugated molecular wires, we begin with the prototypical single molecule junctions, benzenedithiol (BDT)-Au and benzenediamine (BDA)-Au junctions.

Conductance of BDT-Au junctions in units of G_0			
DFT	DFT+Σ	GW	Experiment
0.29 [54]	0.01 [129]	0.01 (BDT+H) [61]	$5.8x10^{-4}$ [18]
0.067-0.57 [56]		0.83 (BDT) [61]	0.011 [19]
0.1-0.2 [55]			0.01 (LC), 0.1 (HC) [130]
0.4-0.9 [57]			$5x10^{-5}$ [131]
0.38 [78]			0.011 [132]
0.24 [133]			0.005 [23]
0.04 [129]			
Conductance of BDA-Au junctions in units of G_0			
DFT	DFT+Σ	GW	Experiment
0.046 [58]	0.005 [11]	0.0042 [61]	0.0064 [26]
			0.01 [23]

Table 3. Experimental and theoretical conductance values of benzenedithiol-Au and benzenediamine-Au junctions. HC and LC corresponds to the high conductance and low conductance values respectively.

For BDT-Au, conductance values spanning several orders of magnitude from $5x10^{-5}G_0$ to $0.1G_0$ were reported from earlier experiments [18, 19, 130, 131], while recent measurements have settled to more consistent values ranging between 0.005-0.01 G_0 [23, 132]. On the theoretical front, many authors have performed DFT calculations on BDT-Au junctions, giving conductances in the range of $0.067\text{-}0.9G_0$. It was also found from DFT calculations that the conductance is strongly dependent on the binding geometry, similar to the alkanethiol-Au case, and typical for Au-thiol contacted systems [56, 57]. This finding is consistent with the large range of experimental conductance values. A GW transport calculation for BDT-Au junctions with the Sulfur attached to flat Au surfaces gave a conductance value of $0.83G_0$, much larger than experimentally measured values. However, a similar calculation with benzene-dithiolate (BDT+H) on

pyramidal Au contacts gives a reasonable conductance value of 0.01 G_0. More recently, a DFT+Σ calculation for BDT attached to Au pyramidal contacts also gave a conductance of 0.01 G_0 [129].

For better comparison between theory and experiments, junctions containing benzenediamine have been considered, as amine end-groups are found experimentally to have less variability in conductance [20, 23, 26, 134]. Experiments on BDA-Au junctions report conductance values between 0.005-0.01 G_0 [23, 26], while DFT calculations predict a significantly larger value of 0.046 G_0 [58]. Inclusion of GW corrections lowers the conductance to 0.0042 G_0 and brings it much closer to the experimental range [61]. Similarly, DFT+Σ calculations have yielded a value of 0.005 G_0, in agreement with experimental measurements and GW calculated values [11]. The conductance of BDA molecules was further investigated by chemical functionalization. Experimentally, the conductance of BDA was varied between 5.5 x10^{-3} G_0 and 8.2x10^{-3} G_0 by substituting H atoms on the phenyl ring with a series of electron-donating/withdrawing functional groups [24]. By performing DFT+GW and DFT+Σ calculations on these molecules, it was found that both methods yield conductances in good agreement with experiments. However, DFT+Σ predicts conductances that are closer to the measured values while GW calculations give better conductance trends across various functional groups [85].

In addition to amines, other anchoring groups such as pyridine have also been found to have less variability in conductance and therefore more suitable for benchmark studies [20, 35, 58]. Through a combined experimental and theoretical analysis [35], it was found that the conductance histogram in pyridine-Au junctions have two conductance peaks (the high-G and low-G peaks), corresponding to two different molecular geometries. The low-G geometry has the molecular backbone aligned perpendicular to the metal surface, while the high-G geometry has molecules tilted in the junction between the metal electrodes.

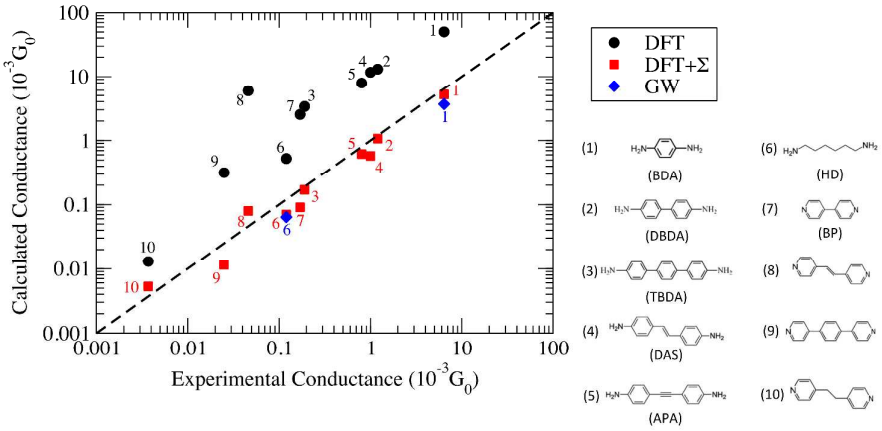

Figure 5. Conductance obtained from DFT (black circles), DFT+Σ (red squares), and GW (blue diamonds) plotted against experimental conductances on a log-log scale for Au junctions containing (1) 1,4-benzenediamine (BDA), (2) 4,4'-dibenzenediamine (DBDA), (3) 4,4''-tribenzenediamine (TBDA), (4) 4,4′-diamino-stilbene (DAS), (5) bis-(4-aminophenyl)acetylene (APA), (6) 1,6-hexanediamine (HDA), (7) 4,4′-bipyridine (BP),

(8) 1,2-bis(4-pyridyl)ethylene, (9) 4,4′′-bis(4-terpyridine), and (10) 1,2-bis(4-pyridyl)ethane. DFT, DFT+Σ, and experimental results for molecules 1-3 are obtained from Refs. [11, 26], molecules 4-6 from Refs. [135, 136], and molecules 7-10 from Ref. [89] (low G values). GW results are obtained from Refs. [85, 137].

In Figure 5, the zero-bias conductance data from calculations and experiments are plotted for a number of junctions with amine and pyridine terminated molecules sandwiched between Au-leads. From this plot, it is obvious that DFT substantially over-estimates the electron conductance relative to experimental values while both DFT+Σ and GW give much better agreement with experiment. In addition to overestimating the conductance, DFT can also yield incorrect conductance trends. For example, the conductance of BP-Au junctions (molecule 7) is smaller than that of 1,2-bis(4-pyridyl)ethylene-Au junctions (molecule 8) within DFT, while DFT+Σ correctly predicts a larger conductance for BP relative to molecule 8 in agreement with experiment.

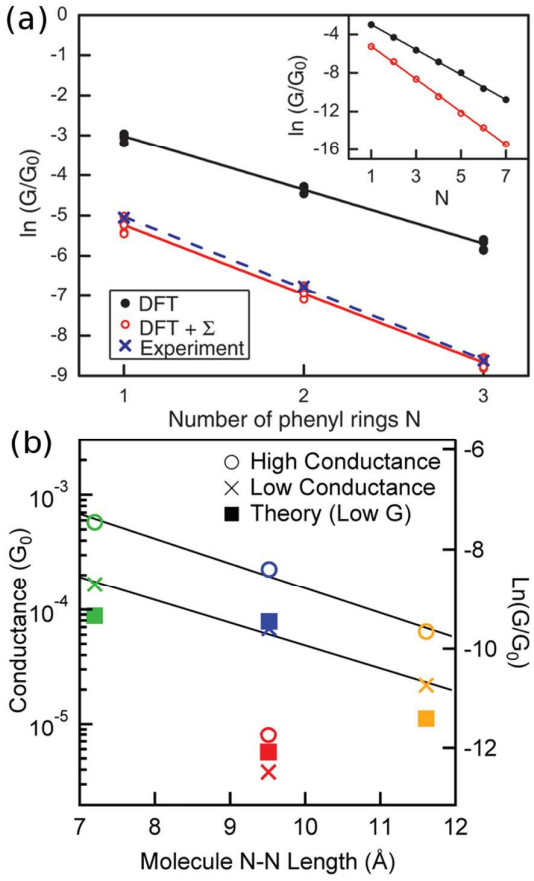

Figure 6. (a) Plot of logarithmic conductance against the number of rings for oligophenyldiamine junctions. N equals 1, 2 and 3 correspond to one, two and three phenyl rings respectively. Inset: Calculated conductance of N up to 7. (b) Similar plot for a number of pyridine junctions. Color legends: Green (molecule 7), Blue (molecule 8), Orange (molecule 9), Red (molecule 10), following the numbering scheme in Figure 5.

(Panel (a) is reproduced by permission of the American Chemical Society (ref. [11])). (Panel (b) is reproduced by permission of the American Chemical Society (ref. [89])).

Now we consider the exponential decay constant β in molecular wires of oligophenyldiamine-Au junctions as well as wires based on pyridine-Au junctions. Although errors for β are not as dramatic as for G, at a quantitative level, DFT Landauer calculations still under-estimate its magnitude relative to experiments in the case of oligophenyldiamine-Au junctions. Figure 6(a) shows a plot of $\ln(G/G_0)$ against the number of phenyl rings N for oligophenyldiamine molecular junctions. Here DFT+Σ predicts a decay constant β equal to 1.7 per phenyl ring and experiments yield a value of 1.7±0.1 per ring, while DFT under-estimates β to be 1.3 per ring [11, 26]. These results show that the DFT+Σ method predicts both G and β that are in agreement with experiments, and a proper inclusion of self-interaction corrections is necessary for the successful prediction of these quantities.

The same exponentially decaying behavior of conductance with length is found for a number of pyridine-terminated aromatic molecular junctions, as shown in Figure 6(b). Molecule 10 is orders of magnitude less conductive than the other molecules being considered because of conjugation breaking at the C-C single bond. The experimentally determined decay constants are ~ 0.5/Å for both low and high G junctions of molecules 7-9. Experimental histograms show that the high conductance plateaus are more complicated than the low G ones, indicative of variability in the junction geometries. On the other hand, DFT+Σ correctly predicts the conductance of the low G series and its length dependence, as shown in Figure 6(b). An eigenchannel analysis shows that electron transmission through these conjugated molecules are dominated by the LUMO level with π* character on the pyridine rings. This explains the relatively small decay constant observed in experiments. --

While we have shown some representative results from the literature, comparing the predicted value of conductance with experiment still requires sampling a significant number of geometries. Generally, the DFT+Σ predicted value of conductance falls within the experimentally measured range (given by the full-width-at-half-maximum of the conductance histogram). Since conductance of individual junctions depends on the specific contact geometry, one has to be careful about quantitative comparisons of predicted β values with the experimentally determined β. This is because the experimentally determined β is obtained from the conductance histogram peaks for molecules of different lengths, but molecules of different lengths could conceivably have very different contact geometries. At present, a proper prediction of contact geometry as a function of molecular length is still beyond computational means. Instead, typically, an unbiased prediction of β will use very similar models of the contact geometry for molecules of different lengths. In Figure 7, we plot in detail the conductance values for different contact geometries used to obtain the β value in Figure 6(a). From Figure 7, we see that the β value obtained from considering all data points is almost the same as that obtained by considering data points for different lengths using the same contact geometry. However, if one were to pick Geometry 5 for N = 1 and Geometry 1 for N = 3, the predicted β value would be quite different. The variability of contact geometry with molecule length in experiment is likely to be the reason for the discrepancy between

experiment and DFT+Σ values for β in oligophenyl-diamine-Ag junctions [11, 109]. Indeed, the variation in conductance upon junction elongation is found to be larger for Ag junctions than for Au junctions, leading to sloped conductance plateaus and broader peaks in the conductance histograms [109]. This has been shown to result from a larger sensitivity of electronic coupling to details of the Ag-N binding geometry [109].

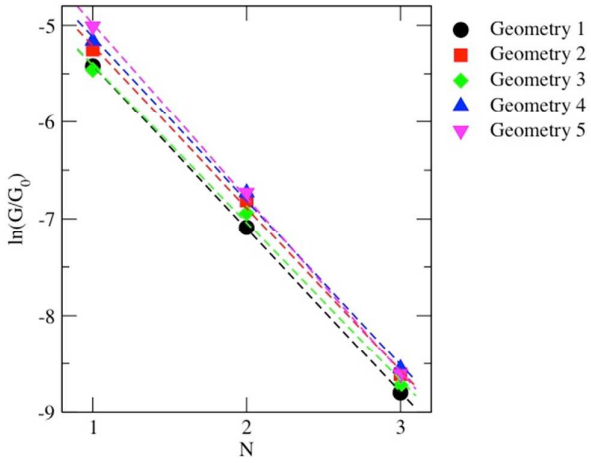

Figure 7. Plot of logarithmic conductance against the number of rings for oligophenyldiamine junctions with different contact geometries. *N* equals 1, 2 and 3 correspond to one, two and three phenyl rings respectively.

3.2.2 Thermopower

Single-molecular junctions possess a large phonon mode mismatch at the metal-molecular interface and tunable electronic conductance properties, making them promising candidates for potential nanoscale thermoelectric applications [138-140]. Recent experiments demonstrated direct measurement of thermopower (i.e., Seebeck coefficient) [45] as well as concurrent measurement of electronic conductance and thermopower [46] for various single-molecular junctions. The thermopower S is an important transport property that gives us information not available from electron conductance measurements, such as the charge carrier type and thermoelectric responses. By combining experiments with model theories or first principles calculations, important molecular junction characteristics such as electronic level alignment and coupling strengths Γ can be inferred accordingly [141].

From Equation (4) in Section 2.2, it is clear that thermopower S is an intensive quantity, proportional to the logarithmic derivative of the electron transmission at the Fermi level E_F. If the transmission near the Fermi level is dominated by off-resonant tunneling, thus showing an exponential decay with the number of molecular units $\tau(E) = A(E)\exp(-\beta(E)N)$, equation (4) implies that the thermopower S depends linearly on N with the linear slope given by

$$\beta^S = S_0(\partial(\beta_N(E))/(\partial E))|_{E=E_F} \quad (9).$$

Because thermopower S arises from an imbalance of charge carriers close to E_F, a positive S implies that hole transport is dominant near E_F, while a negative S implies that electron transport is dominant. Often, this concept is extended to conclude that a positive S implies HOMO-dominated transport, while a negative S implies LUMO-dominated transport, by using a Lorentzian function to approximate the transmission function. Likewise, within the Lorentzian model, a positive (negative) β^S implies HOMO (LUMO)-dominated transport. However, in the case of molecular junctions, interface states can result in non-Lorentzian transmission functions[46], changing the gradient of transmission significantly, thus underscoring the importance of both first principles calculations and experiments in understanding the thermopower in these systems.

To illustrate the relevance and importance of interface states in thermopower measurements, we consider the case of oligophenyldiamine-Au junctions. DFT and DFT+Σ calculations were performed for these junctions, with different number of phenyl rings in the molecule [95]. Two contact geometries were considered, with amine binding to single Au adatoms on Au(111), or a trimer of three Au atoms on Au(111). Au d-orbital derived interface states result in highly non-Lorentzian transmission functions close to E_F for the adatom case; on the other hand, the transmission function is quite smooth close to E_F for the trimer case. Since S is sensitive to the gradient of transmission close to E_F, the derived values of S are quite different for the adatom and trimer cases, although the computed values of β^S were almost the same for the two contact geometries [95]. Interestingly, the experiment by Segalman *et al.* gave S values that are in excellent agreement with the DFT+Σ values for the trimer case, while the experiment by Venkataraman *et al.* [46] gave S values in good agreement with the DFT+Σ values for the adatom case. This is consistent with the fact that the experiments by Segalman *et al.* probe the thermopower of molecular junctions without crashing the scanning tunneling microscope (STM) tip into the Au surface (thus leaving a relatively smooth Au surface), whereas the experiments by Venkataraman *et al.* probe the thermopower of single molecule junctions obtained by first crashing the STM tip into the Au surface to form a rough surface. Regardless of the experimental details, the DFT+Σ values of S are within the full-width half-maximum in experiments, while the DFT values are too large [95]. This discussion underscores the need to consider interface states in interpreting thermopower measurements, while also emphasizing the importance of proper energy level alignments in first principles transport calculations for S.

We now summarize the key results for the length dependence of thermopower in molecular junctions [40, 45, 95, 142], where interface states can at times lead to an unexpected sign for β^S [142]. Specifically, it was found that thermopower S increases linearly with length for oligophenyldiamines and oligophenyldithiols, but decreases linearly with length for alkanedithiols. The former behavior is understood as HOMO dominated tunneling in which the HOMO resonance moves closer to E_F with increasing length for conjugated systems, while the latter is attributed to the presence of metal-induced gap states between the HOMO and LUMO levels.[142] On the other hand, for highly conducting Au-C linked junctions, the thermopower S is found to increase non-linearly with length and saturate for oligophenyls, but to remain constant with length for alkanes [40]. Comparison of computed β^S values for oligophenyldiamine-Au

junctions with experiments showed that DFT overestimates this quantity, while DFT+Σ gives values in agreement with experiment [95].

Numerical convergence of the thermopower S with respect to the sampling density of $k_{//}$ is significantly more challenging than that for the conductance, especially when interface states affect the transmission spectra [95]. Nevertheless, several GW calculations have been performed to compute the thermopower of single molecule junctions. In Table 4, we present the predicted values of S for different molecules, using DFT, DFT+Σ and GW methods, and compare the results with experiment. In general, DFT overestimates the magnitude of the thermopower, while both DFT+Σ and GW give better agreement with experiment. In addition, S.-H. Ke *et al*. [143] used a DFT single particle Green's function method with the hybrid B3LYP and PBE0 exchange-correction functional to study the thermopower of a range of molecular junctions. They were able to get very good quantitative agreement of thermopower compared with experiments, but the predicted electronic conductance under the same framework is still over-estimated.

Molecule	DFT	DFT+Σ	GW	Experiment
Benzenediamine	12.3[a];	3.9[a];	7.8[b];	2.3±0.3[c];
Benzenedithiol	7.49[d]; 6.4[g];	2.4[g];		7.2±0.2[e]; 8.7±2.1[f];
Benzenedicyanide	-69.9[g];	-11.5[g];	-9.2[b];	-1.3±0.5[e];
Biphenyldiamine	17.9[a];	5.4[a];		4.9±1.9[c];
Triphenyldiamine	24.3[a];	8.1[a];		6.4±0.4[c];
4,4'-bipyridine	-38.17[h];	-7.88[h];		-9.5[h];
B4APA	2.8[i];	4.71[h]; 0.9~1.1[i];	11.6[i];	9.7±0.3[h];

Table 4: Thermopower (μV/K) of various molecular wire junctions connected by gold electrodes at room temperature. B4APA = bis-(4-aminophenyl) acetylene. Benzene derivatives are anchored at 1,4 position. 4,4'-bipyridine is showing data for high-conductance configuration. Data are from a: Ref. [95]; b: Ref. [86]; c: Ref. [142]; d: Ref. [144]; e: Ref. [145]; f: Ref. [45]; g: Ref. [129]; h: Ref. [46]; i: Ref. [146].

In general, getting good agreement between theory and experiment for both thermopower and conductance is still a challenge for many molecules. Yet, the agreement that has been achieved thus far, with DFT+Σ [95, 141] and GW [146] approaches, gives clear evidence of the validity of off-resonant tunneling transport in

these single-molecule junctions. On the other hand, it is interesting to highlight one particularly simple case: that of pyridine-Au junctions, where the LUMO-derived transmission can be well described by a simple Lorentzian function. Accordingly, Lorentzian models can be used to derive the level alignments and lead-molecule coupling from simultaneously measured values of S and G in pyridine-Au junctions, and this has been shown to agree well with DFT+ Σ results [141].

4. Towards Perfect Molecular Wires

A one-dimensional (1D) metal tends to slightly rearrange the atomic positions to gain electronic energy at the price of elastic energy associated with lattice distortion. This Peierls distortion effect opens a gap in most 1D wires such as polyacetylene, and armchair graphene nanoribbons (AGNRs) [147], therefore transport through these semiconducting 1D or quasi-1D wires has to occur via the tunneling or hopping mechanisms. Even so-called metallic carbon nanotubes typically have a very small band gap due to curvature and strain effects [148, 149]. Within the tunneling regime, the low-bias conductance G of a molecular wire decays exponentially with length, and high performance molecular wires are characterized by a large contact conductance G_C and small decay constant β. In general, as the Fermi level approaches the frontier orbitals, G_C increases and approaches its peak value at resonance while β decreases.

So far, there have been many experimental and theoretical efforts devoted to understanding the factors determining β in the search for high performance molecular wires. Table 5 lists the experimentally measured and theoretically calculated β and G_C values for many different types of molecular wires.

Molecule	Link group	β (Å^{-1})	G_C (G_0)
extended viologen molecules [150]	S	0.006 ± 0.0004	8.4×10^{-5}
oligoporphyrins containing coordinated zinc cations [151]	Thioacetates	0.04 ± 0.006	8.6×10^{-5}
OPEs	Carbodithioate [152]	0.05	7×10^{-3}
	Thiol [152-155]	0.2 – 0.34	10^{-3}
[3xn] gold-ion clusters enclosed within self-assembled cages [156]	Panel ligands	0.05 (DFT: 0.02)	1.1×10^{-2}
Oligoynes	Py = 4-pyridyl	0.06 ± 0.03 [157]	2×10^{-4} (LC), 6×10^{-4} (MC) [157]
		0.31 ± 0.04 [158]	6.3×10^{-2} [158]
	CN [158]	0.17 ± 0.01	8.1×10^{-4}

	NH_2 [158]	~0.25	4.8×10^{-2}
	BT [158]	0.29 ± 0.02	1.2
	-SH [158]	~0.318	0.96
Oligothiophenes [5]	Thiocyanate group	0.1	1.7×10^{-2}
Benzene-furan oligoaryls [159]	Thiolated (-SH)	0.11-0.13 (conformation by stretching the molecule develops a smaller β)	3.3×10^{-4}
Carotenoid polyenes	Pyridine [160]	0.17 ± 0.03	$(1.8 \pm 1.5) \times 10^{-4}$
	Thiol [161]	0.22 ± 0.04	$(4.8 \pm 2.3) \times 10^{-4}$
Oligophenyleimine (OPI) [41]	S	0.3 (tunnelling regime) 0.09 (hopping regime)	
7-AGNR [162]	No link group	0.45 ± 0.06 (Low bias)	$\sim 10^{-2}$
		0.1 ~ 0.2 (High bias)	$\sim 10^{-2}$
AGNR sheet [163]	zigzag edge atom (gold chain as leads)	Hybrid-DFT: ~ 0.117	Hybrid-DFT: ~ 10^{-3}
AGNR [164]	zigzag edge (wider AGNR as leads)	DFT: ~ 0	DFT: 0-1 tunable with bias
(8,0) CNT [103]		DFT-CBS: ~ 0.12	

Table 5: Experimentally measured and theoretically calculated β and G_C values for different molecular wires. Unless otherwise stated, the wires are coupled to gold electrodes via different link groups. Oligophenyls and alkane chains have been excluded from this table as they have been discussed elsewhere in the text.

We see from the table that there are many organic molecules with very small measured β (< 0.1 Å^{-1}), including oligoynes [157], conjugated porphyrin oligomers [151], and extended viologen molecules [150]. However, many of these systems also have a relatively small conductance, with G ranging between 10^{-5} to 10^{-4} G_0. As can be seen, extended viologen molecules [150] shows one of the smallest β measured, and its conductance is likely to be dominated by the LUMO. There have also been several studies showing that the junction conductances can be strongly affected by the link groups [152, 158, 160, 161]. In particular, the carbodithioate link group is found to lower the effective barrier for charge transport and enhance the conductances by an order of magnitude [152]. In addition, there have also been theoretical predictions that

oligopolyynes [165] and oligoperylenes [166] attached to Au electrodes can have very small β and large G_c values.

Recently, bottom-up synthesis of AGNRs of specific widths has been achieved [162, 167-170], and molecular wires made of AGNRs have been proposed and studied. AGNRs can be classified into three families, according to the number of carbon atoms, n, across the width of the AGNR. The three families are n = 3p, 3p+1 and 3p+2 where p is an integer. Following standard convention, we call an AGNR with n carbon atoms across its width an n-AGNR. A recent report finds that a finite 7-AGNR molecule attached to gold electrodes shows a very low G_C but fast decay rate at low bias. Higher G_C and lower β can be reached as the bias window approaches the delocalized HOMO and LUMO levels [162]. However, if we attach an AGNR segment to gold chains via its zigzag edge at both ends, an unusual exponential increase of transmission with wire length ($\beta = -0.117$ Å^{-1}) has been predicted based on the extended Caroli, Combescot, Nozieres, and Saint-James (CCNS) formulation for tunneling currents with the Hamiltonian derived from hybrid DFT-B3LYP calculations [163, 171]. This phenomena has been attributed to the localization of orbital amplitude at the two zigzag terminations and the remarkable decrease in the HOMO-LUMO gap with molecule length [163].

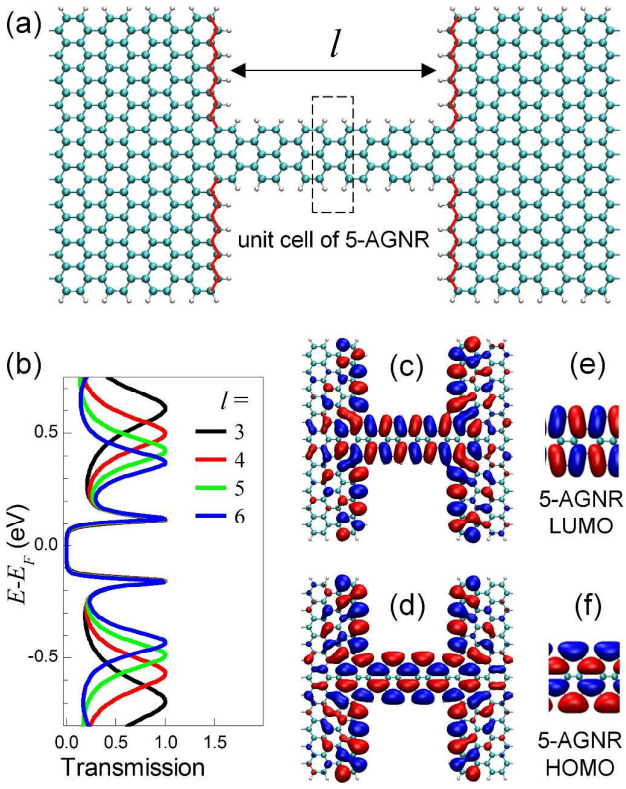

Figure 8. (a) Atomic structure of a 5-AGNR seamlessly attached to wider AGNR leads incorporating zigzag edges at the interface (denoted by red lines). The length of the 5-AGNR segment l = 5 unit cells. (b) Transmission curves of junction shown in (a) with varying l, calculated from first-principles scattering-state approach as implemented in SCARLET [78]. (c-d) Real parts of eigenchannel-wavefunction isosurfaces with isovalue

= +/- 0.025 calculated using SCARLET at the two frontier peaks of the junction with l = 3. (e-f) The Γ-point HOMO and LUMO isosurfaces with isovalue = +/- 0.03 of the perfect 5-AGNR calculated using SIESTA [172].

When a 3p+2-AGNR is seamlessly attached to a wider AGNR leads incorporating zigzag edges at the interface, as shown in Figure 8(a), it is found to show frontier transmission peaks that are almost independent of the wire length (Figure 8(b)) [164]. This length-independence is attributed to special link groups, i.e. the zigzag edges at the interface between the narrower AGNR molecule and wider AGNR leads. Such link groups provide two effects to the frontier peaks. First, they eliminate the confinement effect within the AGNR molecule in the sense that they keep the eigenenergies and eigenchannel wavefunctions of the two frontier resonances similar to that of the infinite AGNR ribbon, independent of the length of the AGNR fragment (see Figure 8(c-f)). This property is related to the fact that the states in the infinite 3p+2-AGNR can match very well to the zigzag edge states without any frustration or distortion. Secondly, these link groups serve as electrons "sources" and "drains" (zigzag edge) that absorb any change in the coupling to the leads as the wire lengthens. Further details can be found in Ref. [164]. In addition to 3p+2-AGNRs, it is also very likely that metallic carbon nanotubes are excellent candidates for perfect molecular wires [173-175].

5. Concluding Remarks

In this review, we have focused on a first principles theory perspective of electron transport through molecular wires, applicable in the off-resonant tunneling regime. We show that complex band structure calculations are helpful to provide a quick estimate of the decay constant beta, but they neglect effects of the metal-molecule geometry, which are significant and need to be considered for quantitative predictions of conductance and beta. The Landauer-Buttiker formalism, which explicitly takes into account contact geometries, is a useful tool to predict conductance, thermopower and beta values in molecular wires. Within this formalism, GW and DFT+Σ calculations can accurately predict conductance values, compared to DFT calculations which tend to overestimate the conductance by orders of magnitude, especially in the off-resonant tunneling regime. The reason for this significant improvement is that off-resonant tunneling conductance is very sensitive to the energy barrier for transport, and only GW and DFT+Σ calculations incorporate accurate values of this energy barrier. DFT+Σ calculations are particularly useful as they are of similar computational expense to DFT calculations, thus allowing a number of different contact geometries to be considered. However, at present, a truly effective search for typical contact geometries in experiment is still elusive due to the large number of atoms involved and the need to consider atomic-scale dynamics. Therefore, while DFT+Σ can give values of conductance close to the peaks in experimental conductance histograms, disagreement between calculated and measured values of beta can arise when the experimental contact geometry changes significantly with molecule length. However, the fact that DFT+Σ can accurately predict not only conductance, but also the thermopower of oligophenyldiamine-Au junctions, provides evidence that transport in these systems occurs via off-resonant tunneling, and sets the framework for a consistent understanding of independent experimental probes of charge transport through these wires.

GW calculations go beyond DFT+Σ by taking into account dynamical effects and is in principle applicable to all classes of systems; therefore, GW is by far the gold standard in terms of making accurate predictions for charge transport in single molecule junctions. However, in practice, the high computational cost of GW restricts this method to relatively small system sizes. Furthermore, very high energy cutoffs and large number of conduction bands are involved in accurately predicting the ionization potential or electron affinity of molecules within GW [176]. This implies that similarly large cutoffs are required to obtain correct level alignments for molecule-metal systems within GW, an issue that is critical for transport calculations.

The present review is not exhaustive, and special mention must be given here to several other topics that we have omitted. In recent years, the study of quantum interference pathways in single molecule junctions has been performed by both experiment and theory, providing yet another confirmation of quantum coherence in these systems [177, 178]. Increasingly sophisticated experiments are being set up to perform vibrational spectroscopy on single molecule junctions, simultaneously to the measurement of conductance and/or thermopower [43]. These experiments would provide valuable information on the contact geometry of the junctions, and can be combined with first principles calculations to directly relate electron transport properties with the atomic structure. Finally, the transport of electron spin in molecular wires has also been studied using DFT [179-181] and DFT+Σ [182] calculations, but so far, there have been no benchmark experiments to compare these results against. In general, spin transport is much more sensitive to details of the interface geometry than non-spin-polarized transport.

Moving forwards, it would be extremely helpful to develop effective classical potentials to treat the interactions between typical metal electrodes and organic molecules. This would be an important step towards using more representative model geometries for transport calculations. Investigating the effects of solvent molecules on transport properties is another important consideration. Furthermore, electron transport through very long molecular wires typically occurs via thermally-activated hopping. To this end, it would be interesting to develop multi-scale methods incorporating first principles theory to compute the conductance. Furthermore, the full power of Marcus theory has yet to be exploited to study hopping transport in open quantum systems of molecular junctions including contact with electron reservoirs.

Acknowledgements

The authors gratefully acknowledge the Singapore National Research Foundation for funding via the NRF Fellowship Grant (NRF-NRFF2013-07).

Biography

Khoong Hong Khoo received her Bachelor's Degree in Physics from the National University of Singapore and Ph.D. from the University of California at Berkeley, where she worked on electronic transport through nanostructures with Prof. Steven G. Louie. She then spent 3 years as a postdoctoral researcher with Prof. James R. Chelikowsky at the University of Texas at Austin before joining the Institute of High Performance Computing in Singapore as a scientist and the National University of Singapore as a Senior Research Fellow working with Su Ying Quek. She is interested in the study of materials using first-principles electronic structure methods.

Yifeng Chen received his B.S. degree in physics from Fudan University, Shanghai in 2008 and his Ph.D. degree in physics from North Carolina State University in May, 2013. He has worked on nanoscale transport and spintronics using computational methods with Prof. Marco Buongiorno Nardelli for his PhD thesis. Since September 2013, he has been a postdoctoral fellow with Prof. Su Ying Quek at the National University of Singapore and the Graphene Research Center and his current research is on computational nanomaterials and related topics.

Suchun Li received her B.Sc. degree in Physics with 1st class Honours from Nanyang Technological University. Upon graduation in 2010, she was awarded the A*STAR Graduate Scholarship and joined the National University of Singapore as a Ph.D. student, working with Prof. Yuan Ping Feng and Prof. Su Ying Quek on the electronic and transport properties of graphene nanoribbons using first-principles calculations. She is expecting to receive her Ph.D. degree soon, and has recently joined the Institute of High Performance Computing as a Scientist.

Su Ying Quek graduated with B.A. Honors (1st class) in Mathematics from the University of Cambridge in 2000 and obtained her Ph.D. in Applied Physics from Harvard University in 2006, working with Efthimios Kaxiras and Cynthia Friend. After a year of exchange studies at University of California, Berkeley, in 2005 with Steven G. Louie, she joined Jeff Neaton in Lawrence Berkeley National Laboratory as his first postdoctoral associate, from 2006 to 2010. From 2011 to 2013, she was an Independent Investigator in the Institute of High Performance Computing, Singapore. In August 2013, she joined the National University of Singapore as an Assistant Professor, supported by the Singapore National Research Foundation Fellowship. Her research interests are in the electronic structure and transport properties of emerging materials.

References

1. Aviram, A. and M.A. Ratner, *MOLECULAR RECTIFIERS.* Chemical Physics Letters, 1974. **29**(2): p. 277-283.
2. Polymeropoulos, E.E. and J. Sagiv, *ELECTRICAL-CONDUCTION THROUGH ADSORBED MONOLAYERS.* Journal of Chemical Physics, 1978. **69**(5): p. 1836-1847.
3. Huber, R., et al., *Electrical conductance of conjugated oligorners at the single molecule level.* Journal of the American Chemical Society, 2008. **130**(3): p. 1080-1084.
4. Cuevas, J.C., et al., *Theoretical description of the electrical conduction in atomic and molecular junctions.* Nanotechnology, 2003. **14**(8): p. R29-R38.
5. Yamada, R., et al., *Electrical conductance of oligothiophene molecular wires.* Nano Letters, 2008. **8**(4): p. 1237-1240.
6. Wang, C., et al., *Oligoyne Single Molecule Wires.* Journal of the American Chemical Society, 2009. **131**(43): p. 15647-15654.
7. Kim, B., et al., *Molecular Tunnel Junctions Based on pi-Conjugated Oligoacene Thiols and Dithiols between Ag, Au, and Pt Contacts: Effect of Surface Linking*

Group and Metal Work Function. Journal of the American Chemical Society, 2011. **133**(49): p. 19864-19877.
8. Porath, D., et al., *Direct measurement of electrical transport through DNA molecules.* Nature, 2000. **403**(6770): p. 635-638.
9. Engelkes, V.B., J.M. Beebe, and C.D. Frisbie, *Length-dependent transport in molecular junctions based on SAMs of alkanethiols and alkanedithiols: Effect of metal work function and applied bias on tunneling efficiency and contact resistance.* Journal of the American Chemical Society, 2004. **126**(43): p. 14287-14296.
10. Sedghi, G., et al., *Long-range electron tunnelling in oligo-porphyrin molecular wires.* Nature Nanotechnology, 2011. **6**(8): p. 517-523.
11. Quek, S.Y., et al., *Length Dependence of Conductance in Aromatic Single-Molecule Junctions.* Nano Letters, 2009. **9**(11): p. 3949-3953.
12. Bujak, P., et al., *Polymers for electronics and spintronics.* Chemical Society Reviews, 2013. **42**(23): p. 8895-8999.
13. Bredas, J.L., et al., *Charge-transfer and energy-transfer processes in pi-conjugated oligomers and polymers: A molecular picture.* Chemical Reviews, 2004. **104**(11): p. 4971-5003.
14. Mann, B. and H. Kuhn, *TUNNELING THROUGH FATTY ACID SALT MONOLAYERS.* Journal of Applied Physics, 1971. **42**(11): p. 4398-&.
15. Polymeropoulos, E.E., D. Mobius, and H. Kuhn, *MONOLAYER ASSEMBLIES WITH FUNCTIONAL UNITS OF SENSITIZING AND CONDUCTING MOLECULAR-COMPONENTS - PHOTO-VOLTAGE, DARK CONDUCTION AND PHOTOCONDUCTION IN SYSTEMS WITH ALUMINUM AND BARIUM ELECTRODES.* Thin Solid Films, 1980. **68**(1): p. 173-190.
16. Fujihira, M., K. Nishiyama, and H. Yamada, *PHOTOELECTROCHEMICAL RESPONSES OF OPTICALLY TRANSPARENT ELECTRODES MODIFIED WITH LANGMUIR-BLODGETT-FILMS CONSISTING OF SURFACTANT DERIVATIVES OF ELECTRON-DONOR, ACCEPTOR AND SENSITIZER MOLECULES.* Thin Solid Films, 1985. **132**(1-4): p. 77-82.
17. Luo, L., S.H. Choi, and C.D. Frisbie, *Probing Hopping Conduction in Conjugated Molecular Wires Connected to Metal Electrodes.* Chemistry of Materials, 2011. **23**(3): p. 631-645.
18. Reed, M.A., et al., *Conductance of a molecular junction.* Science, 1997. **278**(5336): p. 252-254.
19. Xiao, X.Y., B.Q. Xu, and N.J. Tao, *Measurement of single molecule conductance: Benzenedithiol and benzenedimethanethiol.* Nano Letters, 2004. **4**(2): p. 267-271.
20. Venkataraman, L., et al., *Single-molecule circuits with well-defined molecular conductance.* Nano Letters, 2006. **6**(3): p. 458-462.
21. Khoo, K.H., et al., *Contact dependence of the conductance of H-2 molecular junctions from first principles.* Physical Review B, 2008. **77**(11): p. 115326.
22. Jia, C. and X. Guo, *Molecule-electrode interfaces in molecular electronic devices.* Chemical Society Reviews, 2013. **42**(13): p. 5642-5660.
23. Kiguchi, M., et al., *Effect of Anchoring Group Position on Formation and Conductance of a Single Disubstituted Benzene Molecule Bridging Au Electrodes: Change of Conductive Molecular Orbital and Electron Pathway.* Journal of Physical Chemistry C, 2010. **114**(50): p. 22254-22261.
24. Venkataraman, L., et al., *Electronics and chemistry: Varying single-molecule junction conductance using chemical substituents.* Nano Letters, 2007. **7**(2): p. 502-506.
25. Galperin, M., M.A. Ratner, and A. Nitzan, *Inelastic electron tunneling spectroscopy in molecular junctions: Peaks and dips.* Journal of Chemical Physics, 2004. **121**(23): p. 11965-11979.

26. Venkataraman, L., et al., *Dependence of single-molecule junction conductance on molecular conformation.* Nature, 2006. **442**(7105): p. 904-907.
27. Wassel, R.A., et al., *Stochastic variation in conductance on the nanometer scale: A general phenomenon.* Nano Letters, 2003. **3**(11): p. 1617-1620.
28. Fatemi, V., et al., *Environmental Control of Single-Molecule Junction Transport.* Nano Letters, 2011. **11**(5): p. 1988-1992.
29. Capozzi, B., et al., *Tunable Charge Transport in Single-Molecule Junctions via Electrolytic Gating.* Nano Letters, 2014. **14**(3): p. 1400-1404.
30. Xu, B.Q. and N.J.J. Tao, *Measurement of single-molecule resistance by repeated formation of molecular junctions.* Science, 2003. **301**(5637): p. 1221-1223.
31. Li, C., et al., *Charge transport in single Au vertical bar alkanedithiol vertical bar Au junctions: Coordination geometries and conformational degrees of freedom.* Journal of the American Chemical Society, 2008. **130**(1): p. 318-326.
32. Teresa González, M., et al., *Conductance values of alkanedithiol molecular junctions.* New Journal of Physics, 2008. **10**(6): p. 065018.
33. Chen, F., et al., *Effect of anchoring groups on single-molecule conductance: Comparative study of thiol-, amine-, and carboxylic-acid-terminated molecules.* Journal of the American Chemical Society, 2006. **128**(49): p. 15874-15881.
34. Chen, W., et al., *Highly conducting pi-conjugated molecular junctions covalently bonded to gold electrodes.* J Am Chem Soc, 2011. **133**(43): p. 17160-3.
35. Quek, S.Y., et al., *Mechanically controlled binary conductance switching of a single-molecule junction.* Nature Nanotechnology, 2009. **4**(4): p. 230-234.
36. Nozaki, D., et al., *Disorder and dephasing effects on electron transport through conjugated molecular wires in molecular junctions.* Physical Review B, 2012. **85**(15): p. 155327.
37. Qi, Y., et al., *Mechanical and charge transport properties of alkanethiol self-assembled monolayers on a Au(111) surface: The role of molecular tilt.* Langmuir, 2008. **24**(5): p. 2219-2223.
38. Vura-Weis, J., et al., *Crossover from Single-Step Tunneling to Multistep Hopping for Molecular Triplet Energy Transfer.* Science, 2010. **328**(5985): p. 1547-1550.
39. Cheng, Z.L., et al., *In situ formation of highly conducting covalent Au-C contacts for single-molecule junctions.* Nat Nanotechnol, 2011. **6**(6): p. 353-7.
40. Widawsky, J.R., et al., *Length-Dependent Thermopower of Highly Conducting Au-C Bonded Single Molecule Junctions.* Nano Letters, 2013. **13**(6): p. 2889-2894.
41. Choi, S.H., B. Kim, and C.D. Frisbie, *Electrical resistance of long conjugated molecular wires.* Science, 2008. **320**(5882): p. 1482-1486.
42. Hines, T., et al., *Transition from Tunneling to Hopping in Single Molecular Junctions by Measuring Length and Temperature Dependence.* Journal of the American Chemical Society, 2010. **132**(33): p. 11658-11664.
43. Aradhya, S.V. and L. Venkataraman, *Single-molecule junctions beyond electronic transport.* Nature Nanotechnology, 2013. **8**(6): p. 399-410.
44. Lee, W., et al., *Heat dissipation in atomic-scale junctions.* Nature, 2013. **498**(7453): p. 209-+.
45. Reddy, P., et al., *Thermoelectricity in molecular junctions.* Science, 2007. **315**(5818): p. 1568-1571.
46. Widawsky, J.R., et al., *Simultaneous Determination of Conductance and Thermopower of Single Molecule Junctions.* Nano Letters, 2012. **12**(1): p. 354-358.
47. Kim, W.Y., et al., *Application of quantum chemistry to nanotechnology: electron and spin transport in molecular devices.* Chemical Society Reviews, 2009. **38**(8): p. 2319-2333.
48. Galperin, M., A. Nitzan, and M.A. Ratner, *Inelastic effects in molecular junctions in the Coulomb and Kondo regimes: Nonequilibrium equation-of-motion approach.* Physical Review B, 2007. **76**(3).

49. Chen, Y.C., M. Zwolak, and M. Di Ventra, *Inelastic effects on the transport properties of alkanethiols.* Nano Letters, 2005. **5**(4): p. 621-624.
50. Sergueev, N., D. Roubtsov, and H. Guo, *Ab initio analysis of electron-phonon coupling in molecular devices.* Physical Review Letters, 2005. **95**(14): p. 146803.
51. Troisi, A., M.A. Ratner, and A. Nitzan, *Vibronic effects in off-resonant molecular wire conduction.* Journal of Chemical Physics, 2003. **118**(13): p. 6072-6082.
52. Chen, Y.C., M. Zwolak, and M. Di Ventra, *Inelastic current-voltage characteristics of atomic and molecular junctions.* Nano Letters, 2004. **4**(9): p. 1709-1712.
53. Asai, Y., *Theory of inelastic electric current through single molecules.* Physical Review Letters, 2004. **93**(24): p. 246102.
54. Stokbro, K., et al., *Theoretical study of the nonlinear conductance of Di-thiol benzene coupled to Au(111) surfaces via thiol and thiolate bonds.* Computational Materials Science, 2003. **27**(1-2): p. 151-160.
55. Evers, F., F. Weigend, and M. Koentopp, *Conductance of molecular wires and transport calculations based on density-functional theory.* Physical Review B, 2004. **69**(23): p. 235411.
56. Tomfohr, J. and O.F. Sankey, *Theoretical analysis of electron transport through organic molecules.* J Chem Phys, 2004. **120**(3): p. 1542-54.
57. Kondo, H., et al., *Contact-structure dependence of transport properties of a single organic molecule between Au electrodes.* Physical Review B, 2006. **73**(23): p. 235323.
58. Quek, S.Y., et al., *Amine-gold linked single-molecule circuits: Experiment and theory.* Nano Letters, 2007. **7**(11): p. 3477-3482.
59. Hedin, L., *NEW METHOD FOR CALCULATING 1-PARTICLE GREENS FUNCTION WITH APPLICATION TO ELECTRON-GAS PROBLEM.* Physical Review, 1965. **139**(3A): p. A796.
60. Hybertsen, M.S. and S.G. Louie, *ELECTRON CORRELATION IN SEMICONDUCTORS AND INSULATORS - BAND-GAPS AND QUASI-PARTICLE ENERGIES.* Physical Review B, 1986. **34**(8): p. 5390-5413.
61. Strange, M., et al., *Self-consistent GW calculations of electronic transport in thiol- and amine-linked molecular junctions.* Physical Review B, 2011. **83**(11): p. 115108.
62. Darancet, P., et al., *Ab initio GW electron-electron interaction effects in quantum transport.* Physical Review B, 2007. **75**(7): p. 075102.
63. Quek, S.Y. and K.H. Khoo, *Predictive DFT-Based Approaches to Charge and Spin Transport in Single-Molecule Junctions and Two-Dimensional Materials: Successes and Challenges.* Acc Chem Res, 2014.
64. Quek, S.Y.S., D. A.; Choi, H. J.; Louie, S. G.; Neaton J. B., *First-Principles Approach to Charge Transport in Single-Molecule Junctions with Self-Energy Corrections: a "DFT+Sigma Method", in preparation.*
65. Vignale, G. and W. Kohn, *Current-dependent exchange-correlation potential for dynamical linear response theory.* Physical Review Letters, 1996. **77**(10): p. 2037-2040.
66. Sai, N., et al., *Dynamical corrections to the DFT-LDA electron conductance in nanoscale systems.* Physical Review Letters, 2005. **94**(18): p. 186801.
67. Kurth, S. and G. Stefanucci, *Dynamical Correction to Linear Kohn-Sham Conductances from Static Density Functional Theory.* Physical Review Letters, 2013. **111**(3): p. 030601.
68. Di Ventra, M. and T.N. Todorov, *Transport in nanoscale systems: the microcanonical versus grand-canonical picture.* Journal of Physics-Condensed Matter, 2004. **16**(45): p. 8025-8034.
69. Stefanucci, G. and C.O. Almbladh, *Time-dependent quantum transport: An exact formulation based on TDDFT.* Europhysics Letters, 2004. **67**(1): p. 14-20.

70. Varga, K., *Time-dependent density functional study of transport in molecular junctions.* Physical Review B, 2011. **83**(19).
71. Tomfohr, J.K. and O.F. Sankey, *Complex band structure, decay lengths, and Fermi level alignment in simple molecular electronic systems.* Physical Review B, 2002. **65**(24): p. 235105.
72. Tersoff, J., *SCHOTTKY-BARRIER HEIGHTS AND THE CONTINUUM OF GAP STATES.* Physical Review Letters, 1984. **52**(6): p. 465-468.
73. Butcher, P.N., *THERMAL AND ELECTRICAL TRANSPORT FORMALISM FOR ELECTRONIC MICROSTRUCTURES WITH MANY TERMINALS.* Journal of Physics-Condensed Matter, 1990. **2**(22): p. 4869-4878.
74. Paulsson, M. and S. Datta, *Thermoelectric effect in molecular electronics.* Physical Review B, 2003. **67**(24): p. 241403.
75. Malen, J.A., et al., *Fundamentals of energy transport, energy conversion, and thermal properties in organic-inorganic heterojunctions.* Chemical Physics Letters, 2010. **491**(4-6): p. 109-122.
76. Brandbyge, M., et al., *Density-functional method for nonequilibrium electron transport.* Physical Review B, 2002. **65**(16): p. 165401.
77. Rocha, A.R., et al., *Spin and molecular electronics in atomically generated orbital landscapes.* Physical Review B, 2006. **73**(8): p. 085414.
78. Choi, H.J., M.L. Cohen, and S.G. Louie, *First-principles scattering-state approach for nonlinear electrical transport in nanostructures.* Physical Review B, 2007. **76**(15): p. 155420.
79. Choi, H.J. and J. Ihm, *Ab initio pseudopotential method for the calculation of conductance in quantum wires.* Physical Review B, 1999. **59**(3): p. 2267-2275.
80. Liu, S., Y.P. Feng, and C. Zhang, *Communication: Electronic and transport properties of molecular junctions under a finite bias: A dual mean field approach.* Journal of Chemical Physics, 2013. **139**(19).
81. Perdew, J.P., M. Emzerhof, and K. Burke, *Rationale for mixing exact exchange with density functional approximations.* Journal of Chemical Physics, 1996. **105**(22): p. 9982-9985.
82. Becke, A.D., *DENSITY-FUNCTIONAL THERMOCHEMISTRY .3. THE ROLE OF EXACT EXCHANGE.* Journal of Chemical Physics, 1993. **98**(7): p. 5648-5652.
83. Perdew, J.P. and A. Zunger, *SELF-INTERACTION CORRECTION TO DENSITY-FUNCTIONAL APPROXIMATIONS FOR MANY-ELECTRON SYSTEMS.* Physical Review B, 1981. **23**(10): p. 5048-5079.
84. Strange, M. and K.S. Thygesen, *Towards quantitative accuracy in first-principles transport calculations: The GW method applied to alkane/gold junctions.* Beilstein J Nanotechnol, 2011. **2**: p. 746-54.
85. Jin, C.J., et al., *Energy level alignment and quantum conductance of functionalized metal-molecule junctions: Density functional theory versus GW calculations.* Journal of Chemical Physics, 2013. **139**(18): p. 184307.
86. Markussen, T., C. Jin, and K.S. Thygesen, *Quantitatively accurate calculations of conductance and thermopower of molecular junctions.* Physica Status Solidi B-Basic Solid State Physics, 2013. **250**(11): p. 2394-2402.
87. Strange, M. and K.S. Thygesen, *Image-charge-induced localization of molecular orbitals at metal-molecule interfaces: Self-consistent GW calculations.* Physical Review B, 2012. **86**(19): p. 195121.
88. Jin, C. and K.S. Thygesen, *Dynamical image-charge effect in molecular tunnel junctions: Beyond energy level alignment.* Physical Review B, 2014. **89**(4): p. 041102.
89. Kamenetska, M., et al., *Conductance and Geometry of Pyridine-Linked Single-Molecule Junctions.* Journal of the American Chemical Society, 2010. **132**(19): p. 6817-6821.

90. Neaton, J.B., M.S. Hybertsen, and S.G. Louie, *Renormalization of molecular electronic levels at metal-molecule interfaces.* Physical Review Letters, 2006. **97**(21): p. 216405.
91. Biller, A., et al., *Electronic level alignment at a metal-molecule interface from a short-range hybrid functional.* Journal of Chemical Physics, 2011. **135**(16): p. 164706.
92. Garcia-Lastra, J.M., et al., *Polarization-induced renormalization of molecular levels at metallic and semiconducting surfaces.* Physical Review B, 2009. **80**(24): p. 245427.
93. Jain, M., J.R. Chelikowsky, and S.G. Louie, *Reliability of Hybrid Functionals in Predicting Band Gaps.* Physical Review Letters, 2011. **107**(21): p. 216806.
94. Dell'Angela, M., et al., *Relating Energy Level Alignment and Amine-Linked Single Molecule Junction Conductance.* Nano Letters, 2010. **10**(7): p. 2470-2474.
95. Quek, S.Y., et al., *Thermopower of Amine - Gold-Linked, Aromatic Molecular Junctions from First Principles.* Acs Nano, 2011. **5**(1): p. 551-557.
96. Perrin, M.L., et al., *Large tunable image-charge effects in single-molecule junctions.* Nature Nanotechnology, 2013. **8**(4): p. 282-287.
97. Lam, S.C. and R.J. Needs, *1ST-PRINCIPLES CALCULATIONS OF THE SCREENING OF ELECTRIC-FIELDS AT THE ALUMINUM (111) AND (110) SURFACES.* Journal of Physics-Condensed Matter, 1993. **5**(14): p. 2101-2108.
98. McDermott, S., et al., *Tunnel Currents across Silane Diamines/Dithiols and Alkane Diamines/Dithiols: A Comparative Computational Study.* Journal of Physical Chemistry C, 2009. **113**(2): p. 744-750.
99. Picaud, F., et al., *Complex band structures and decay length in polyethylene chains.* Journal of Physics-Condensed Matter, 2003. **15**(22): p. 3731-3740.
100. Li, J., J.K. Tomfohr, and O.F. Sankey, *Theoretical study of carotene as a molecular wire.* Physica E: Low-dimensional Systems and Nanostructures, 2003. **19**(1-2): p. 133-138.
101. Wang, H., J.P. Lewis, and O.F. Sankey, *Band-gap tunneling states in DNA.* Physical Review Letters, 2004. **93**(1): p. 016401.
102. Fagas, G., A. Kambili, and M. Elstner, *Complex-band structure: a method to determine the off-resonant electron transport in oligomers.* Chemical Physics Letters, 2004. **389**(4-6): p. 268-273.
103. Pomorski, P., C. Roland, and H. Guo, *Quantum transport through short semiconducting nanotubes: A complex band structure analysis.* Physical Review B, 2004. **70**(11): p. 115408.
104. Ferretti, A., et al., *Ab initio complex band structure of conjugated polymers: Effects of hydrid density functional theory and GW schemes.* Physical Review B, 2012. **85**(23): p. 235105.
105. Xu, B. and N.J. Tao, *Measurement of single-molecule resistance by repeated formation of molecular junctions.* Science, 2003. **301**(5637): p. 1221-3.
106. Li, X.L., et al., *Conductance of single alkanedithiols: Conduction mechanism and effect of molecule-electrode contacts.* Journal of the American Chemical Society, 2006. **128**(6): p. 2135-2141.
107. Prodan, E. and R. Cart, *Tunneling conductance of amine-linked alkyl chains.* Nano Letters, 2008. **8**(6): p. 1771-1777.
108. Wold, D.J., et al., *Distance dependence of electron tunneling through self-assembled monolayers measured by conducting probe atomic force microscopy: Unsaturated versus saturated molecular junctions.* Journal of Physical Chemistry B, 2002. **106**(11): p. 2813-2816.
109. Kim, T., et al., *Conductance of molecular junctions formed with silver electrodes.* Nano Lett, 2013. **13**(7): p. 3358-64.
110. Thygesen, K.S. and K.W. Jacobsen, *Conduction mechanism in a molecular hydrogen contact.* Physical Review Letters, 2005. **94**(3): p. 4.

111. Marchenkov, A., et al., *Atomic dimer shuttling and two-level conductance fluctuations in Nb nanowires.* Physical Review Letters, 2007. **98**(4): p. 4.
112. Toher, C. and S. Sanvito, *Efficient atomic self-interaction correction scheme for nonequilibrium quantum transport.* Physical Review Letters, 2007. **99**(5): p. 056801.
113. Ke, S.-H., H.U. Baranger, and W. Yang, *Role of the exchange-correlation potential in ab initio electron transport calculations.* Journal of Chemical Physics, 2007. **126**(20): p. 201102.
114. Cehovin, A., et al., *Role of the virtual orbitals and HOMO-LUMO gap in mean-field approximations to the conductance of molecular junctions.* Physical Review B, 2008. **77**(19): p. 195432.
115. Delaney, P. and J.C. Greer, *Correlated electron transport in molecular electronics.* Physical Review Letters, 2004. **93**(3): p. 036805.
116. Baldea, I. and H. Koeppel, *Electron transport through correlated molecules computed using the time-independent Wigner function: Two critical tests.* Physical Review B, 2008. **78**(11): p. 115315.
117. Rangel, T., et al., *Transport properties of molecular junctions from many-body perturbation theory.* Physical Review B, 2011. **84**(4): p. 045426.
118. Hu, Y.B., et al., *Conductance of an ensemble of molecular wires: A statistical analysis.* Physical Review Letters, 2005. **95**(15): p. 4.
119. Basch, H., R. Cohen, and M.A. Ratner, *Interface geometry and molecular junction conductance: Geometric fluctuation and stochastic switching.* Nano Letters, 2005. **5**(9): p. 1668-1675.
120. Muller, K.H., *Effect of the atomic configuration of gold electrodes on the electrical conduction of alkanedithiol molecules.* Physical Review B, 2006. **73**(4): p. 045403.
121. Kaun, C.C. and H. Guo, *Resistance of alkanethiol molecular wires.* Nano Letters, 2003. **3**(11): p. 1521-1525.
122. Fagas, G., P. Delaney, and J.C. Greer, *Independent particle descriptions of tunneling using the many-body quantum transport approach.* Physical Review B, 2006. **73**(24): p. 241314.
123. Lee, M.H., G. Speyer, and O.F. Sankey, *Electron transport through single alkane molecules with different contact geometries on gold.* physica status solidi (b), 2006. **243**(9): p. 2021-2029.
124. Paulsson, M., et al., *Conductance of Alkanedithiol Single-Molecule Junctions: A Molecular Dynamics Study.* Nano Letters, 2009. **9**(1): p. 117-121.
125. Haiss, W., et al., *Anomalous length and voltage dependence of single molecule conductance.* Phys Chem Chem Phys, 2009. **11**(46): p. 10831-8.
126. Fujihira, M., et al., *Currents through single molecular junction of Au/hexanedithiolate/Au measured by repeated formation of break junction in STM under UHV: Effects of conformational change in an alkylene chain from gauche to trans and binding sites of thiolates on gold.* Physical Chemistry Chemical Physics, 2006. **8**(33): p. 3876.
127. Nishikawa, A., et al., *Accurate determination of multiple sets of single molecular conductance of Au/1,6-hexanedithiol/Au break junctions by ultra-high vacuum-scanning tunneling microscope and analyses of individual current-separation curves.* Nanotechnology, 2007. **18**(42): p. 424005.
128. Cheng, Z.L., et al., *In situ formation of highly conducting covalent Au-C contacts for single-molecule junctions.* Nature Nanotechnology, 2011. **6**(6): p. 353-357.
129. Zotti, L.A., et al., *Heat dissipation and its relation to thermopower in single-molecule junctions.* New Journal of Physics, 2014. **16**: p. 25.
130. Tsutsui, M., et al., *High-conductance states of single benzenedithiol molecules.* Applied Physics Letters, 2006. **89**(16).

131. Loertscher, E., H.B. Weber, and H. Riel, *Statistical approach to investigating transport through single molecules.* Physical Review Letters, 2007. **98**(17): p. 176807.
132. Tsutsui, M., M. Taniguchi, and T. Kawai, *Atomistic Mechanics and Formation Mechanism of Metal-Molecule-Metal Junctions.* Nano Letters, 2009. **9**(6): p. 2433-2439.
133. Strange, M., et al., *Benchmark density functional theory calculations for nanoscale conductance.* Journal of Chemical Physics, 2008. **128**(11).
134. Hybertsen, M.S., et al., *Amine-linked single-molecule circuits: systematic trends across molecular families.* Journal of Physics-Condensed Matter, 2008. **20**(37): p. 14.
135. Widawsky, J.R., et al., *Measurement of voltage-dependent electronic transport across amine-linked single-molecular-wire junctions.* Nanotechnology, 2009. **20**(43): p. 434009.
136. Darancet, P., et al., *Quantitative Current-Voltage Characteristics in Molecular Junctions from First Principles.* Nano Letters, 2012. **12**(12): p. 6250-6254.
137. Strange, M. and K.S. Thygesen, *Towards quantitative accuracy in first-principles transport calculations: The GW method applied to alkane/gold junctions.* Beilstein Journal of Nanotechnology, 2011. **2**: p. 746-754.
138. Wang, R.Y., R.A. Segalman, and A. Majumdar, *Room temperature thermal conductance of alkanedithiol self-assembled monolayers.* Applied Physics Letters, 2006. **89**(17): p. 3.
139. Mahan, G.D. and J.O. Sofo, *The best thermoelectric.* Proceedings of the National Academy of Sciences of the United States of America, 1996. **93**(15): p. 7436-7439.
140. Humphrey, T.E. and H. Linke, *Reversible thermoelectric nanomaterials.* Physical Review Letters, 2005. **94**(9): p. 096601.
141. Kim, T., et al., *Determination of Energy Level Alignment and Coupling Strength in 4,4 '-Bipyridine Single-Molecule Junctions.* Nano Letters, 2014. **14**(2): p. 794-798.
142. Malen, J.A., et al., *Identifying the Length Dependence of Orbital Alignment and Contact Coupling in Molecular Heterojunctions.* Nano Letters, 2009. **9**(3): p. 1164-1169.
143. Ke, S.-H., et al., *Thermopower of Molecular Junctions: An ab Initio Study.* Nano Letters, 2009. **9**(3): p. 1011-1014.
144. Pauly, F., J.K. Viljas, and J.C. Cuevas, *Length-dependent conductance and thermopower in single-molecule junctions of dithiolated oligophenylene derivatives: A density functional study.* Physical Review B, 2008. **78**(3): p. 035315.
145. Baheti, K., et al., *Probing the chemistry of molecular heterojunctions using thermoelectricity.* Nano Letters, 2008. **8**(2): p. 715-719.
146. Jin, C.J., T. Markussen, and K.S. Thygesen, *Simultaneous description of conductance and thermopower in single-molecule junctions from many-body ab initio calculations.* Physical Review B, 2014. **90**(7): p. 8.
147. Son, Y.-W., M.L. Cohen, and S.G. Louie, *Energy gaps in graphene nanoribbons.* Physical Review Letters, 2006. **97**(21): p. 216803.
148. Biercuk, M.J.I., S.; Marcus, C. M.; McEuen, P. L., *Electrical Transport in Single-Wall Carbon Nanotubes*, in *Carbon Nanotubes*, A.D. Jorio, G.; Dresselhaus, M. S., Editor. 2008, Springer Berlin Heidelberg. p. 455-493.
149. Ouyang, M., et al., *Energy gaps in "metallic" single-walled carbon nanotubes.* Science, 2001. **292**(5517): p. 702-705.
150. Kolivoska, V., et al., *Single-Molecule Conductance in a Series of Extended Viologen Molecules.* Journal of Physical Chemistry Letters, 2013. **4**(4): p. 589-595.
151. Sedghi, G., et al., *Single molecule conductance of porphyrin wires with ultralow attenuation.* Journal of the American Chemical Society, 2008. **130**(27): p. 8582-+.

152. Xing, Y.J., et al., *Optimizing Single-Molecule Conductivity of Conjugated Organic Oligomers with Carbodithioate Linkers.* Journal of the American Chemical Society, 2010. **132**(23): p. 7946-7956.
153. Kaliginedi, V., et al., *Correlations between Molecular Structure and Single-Junction Conductance: A Case Study with Oligo(phenylene-ethynylene)-Type Wires.* Journal of the American Chemical Society, 2012. **134**(11): p. 5262-5275.
154. Lu, Q., et al., *From Tunneling to Hopping: A Comprehensive Investigation of Charge Transport Mechanism in Molecular Junctions Based on Oligo(p-phenylene ethynylene)s.* Acs Nano, 2009. **3**(12): p. 3861-3868.
155. Liu, K., et al., *Length dependence of electron conduction for oligo(1,4-phenylene ethynylene)s: A conductive probe-atomic force microscopy investigation.* Journal of Physical Chemistry C, 2008. **112**(11): p. 4342-4349.
156. Kiguchi, M., et al., *Highly Conductive 3 x n Gold-Ion Clusters Enclosed within Self-Assembled Cages.* Angewandte Chemie-International Edition, 2013. **52**(24): p. 6202-6205.
157. Wang, C.S., et al., *Oligoyne Single Molecule Wires.* Journal of the American Chemical Society, 2009. **131**(43): p. 15647-15654.
158. Moreno-Garcia, P., et al., *Single-Molecule Conductance of Functionalized Oligoynes: Length Dependence and Junction Evolution.* Journal of the American Chemical Society, 2013. **135**(33): p. 12228-12240.
159. Chen, I.W.P., et al., *The effect of molecular conformation on single molecule conductance: measurements of pi-conjugated oligoaryls by STM break junction.* Chemical Communications, 2007(29): p. 3074-3076.
160. Visoly-Fisher, I., et al., *Conductance of a biomolecular wire.* Proceedings of the National Academy of Sciences of the United States of America, 2006. **103**(23): p. 8686-8690.
161. He, J., et al., *Electronic decay constant of carotenoid polyenes from single-molecule measurements.* Journal of the American Chemical Society, 2005. **127**(5): p. 1384-1385.
162. Koch, M., et al., *Voltage-dependent conductance of a single graphene nanoribbon.* Nature Nanotechnology, 2012. **7**(11): p. 713-717.
163. Tada, T. and K. Yoshizawa, *Reverse exponential decay of electrical transmission in nanosized graphite sheets.* Journal of Physical Chemistry B, 2004. **108**(23): p. 7565-7572.
164. Li, S., et al., *Anomalous length-independent frontier resonant transmission peaks in armchair graphene nanoribbon molecular wires.* Carbon, 2014. **76**(0): p. 285-291.
165. Crljen, Z. and G. Baranovic, *Unusual conductance of polyyne-based molecular wires.* Physical Review Letters, 2007. **98**(11): p. 116801.
166. Bilic, A. and S. Sanvito, *Anomalous length dependence of conductance of aromatic nanoribbons with amine anchoring groups.* Physical Review B, 2012. **86**(12): p. 125409.
167. Cai, J.M., et al., *Atomically precise bottom-up fabrication of graphene nanoribbons.* Nature, 2010. **466**(7305): p. 470-473.
168. Huang, H., et al., *Spatially Resolved Electronic Structures of Atomically Precise Armchair Graphene Nanoribbons.* Scientific Reports, 2012. **2**: p. 983.
169. Linden, S., et al., *Electronic Structure of Spatially Aligned Graphene Nanoribbons on Au(788).* Physical Review Letters, 2012. **108**(21): p. 216801.
170. Yen-Chia Chen, D.G.d.O., Zahra Pedramrazi, Chen Chen, Felix R. Fischer, and Michael F. Crommie, *Tuning the Band Gap of Graphene Nanoribbons Synthesized from Molecular Precursors.* ACS Nano, 2013. **7**(7): p. 6123-6128.
171. C Caroli, R.C., P Nozieres and D Saint-James, *Direct calculation of the tunneling current.* Journal of Physics C: Solid State Physics 1971. **4**.
172. Soler, J.M., et al., *The SIESTA method for ab initio order-N materials simulation.* Journal of Physics-Condensed Matter, 2002. **14**(11): p. 2745-2779.

173. Bachtold, A., et al., *Scanned probe microscopy of electronic transport in carbon nanotubes.* Physical Review Letters, 2000. **84**(26): p. 6082-6085.
174. Tans, S.J., et al., *Individual single-wall carbon nanotubes as quantum wires.* Nature, 1997. **386**(6624): p. 474-477.
175. Mann, D., et al., *Ballistic transport in metallic nanotubes with reliable Pd ohmic contacts.* Nano Letters, 2003. **3**(11): p. 1541-1544.
176. Sharifzadeh, S., et al., *Quantitative molecular orbital energies within a G(0)W(0) approximation.* European Physical Journal B, 2012. **85**(9): p. 323.
177. Aradhya, S.V., et al., *Dissecting Contact Mechanics from Quantum Interference in Single-Molecule Junctions of Stilbene Derivatives.* Nano Letters, 2012. **12**(3): p. 1643-1647.
178. Guedon, C.M., et al., *Observation of quantum interference in molecular charge transport.* Nature Nanotechnology, 2012. **7**(5): p. 304-308.
179. Pilevarshahri, R., et al., *Spin transport in higher n-acene molecules.* Physical Review B, 2011. **84**(17): p. 174437.
180. Bhattacharya, S., A. Akande, and S. Sanvito, *Spin transport properties of triarylamine-based nanowires.* Chemical Communications, 2014. **50**(50): p. 6626-6629.
181. Liang, S.H., et al., *Organic magnetic tunnel junctions: The role of metal-molecule interface.* Physical Review B, 2012. **86**(22): p. 224419.
182. Gorjizadeh, N. and S.Y. Quek, *Interface effects on tunneling magnetoresistance in organic spintronics with flexible amine-Au links.* Nanotechnology, 2013. **24**(41).